# CHARACTERISTICS OF RAYLEIGH WAVE IN THE EPICENTRAL ZONE OF SHALLOW EARTHQUAKE

**A DISSERTATION**

***Submitted in the partial fulfillment of the***

***requirements for the award of the degree***

***of***

**MASTER OF TECHNOLOGY**

**in**

**EARTHQUAKE ENGINEERING**

**(With Specialization in Seismic Vulnerability and Risk Assessment)**

***by***

**SHAILENDRA KUMAR**

**(17553006)**


**DEPARTMENT OF EARTHQUAKE ENGINEERING**

**INDIAN INSTITUTE OF TECHNOLOGY ROORKEE**

**ROORKEE-247 667 (INDIA)**

**JUNE, 2019**

# CANDIDATE'S DECLARATION

I hereby, declare that the work which is being presented in this dissertation entitled, **"CHARACTERISTICS OF RAYLEIGH WAVE IN THE EPICENTRAL ZONE OF SHALLOW EARTHQUAKE"**, being submitted in partial fulfillment of the requirements for the award of degree of "Master of Technology" in "Earthquake Engineering" with specialization in Seismic Vulnerability and Risk Assessment., to the Department of Earthquake Engineering, Indian Institute of Technology Roorkee, under the supervision of Dr. J. P. Narayan, Professor, Department of Earthquake Engineering, Indian Institute of Technology Roorkee, is an authentic record of my own work carried out during the period of June 2018 to June 2019.

I declare that I have not submitted the material embodied in this dissertation for the award of any other degree or diploma.

Place: Roorkee **SHAILENDRA KUMAR**

Date: 17553006

# CERTIFICATE

This is to certify that the above statement made by the candidate is correct to the best of my knowledge and belief.

Place: Roorkee **(Dr. J. P. Narayan)**

Date: Professor

Department of Earthquake Engineering

Indian Institute of Technology Roorkee

# ABSTRACT

The surface waves have more damage potential to both the surface and sub-surface long-span structures as compared to body waves since they can generate large strain in long-span structures in addition to the load reversal. So, there is an urgent need of quantification of characteristics of Rayleigh waves in terms of epicentral distance and focal-depth. In order to fulfill the above identified scientific gaps, the SV-wave responses of a homogeneous half-space model with a sufficient bandwidth in the source time functions (STF) (i.e. Gabor and Ricker wavelets) and various focal depths were simulated and analyzed. Further, the effects of Poisson's ratio and duration of the STF on the characteristics of the generated Rayleigh waves were also studied. The variation of % amount of incident SV-wave energy converted in to the Rayleigh wave energy with focal depth is also quantified.

The analysis of simulated responses revealed generation of Rayleigh wave at the critical distance. The obtained decrease of spectral amplitude and frequency content in the generated Rayleigh waves with an increase of focal depth may be the decrease of curvature of the wave front of the SV-wave. The largest spectral amplitude for unit amplitude of incident SV-wave at the critical distance was obtained in that wavelength for which the ratio of focal depth to wavelength of Rayleigh wave was around 0.63. Further, there is almost exponential decrease of spectral amplitude of Rayleigh wave departing from this constant.

# ACKNOWLEDGEMENT

First appreciation goes to my parents, without whose beliefs, pursuing post-graduation would still have been a dream.

Completion of this dissertation would not have been possible without the expertise of my supervisor **Dr. J. P. Narayan**, Professor in Department of Earthquake Engineering, Indian institute of Technology Roorkee. Frequent discussions throughout the dissertation work were extremely fruitful and helped me to overcome hurdles and problems I faced during this work.

I am highly obliged to **Dr. Neeraj Kumar**, whose timely help and suggestions accelerated the project work. His sincere guidance, encouragement and proper direction gave insight in learning the modelling and understanding the concept in better way.

I am also thankful to **Mr. Lav Joshi** and **Mr. Kavan Modha** for their timely help whenever required.

It will be difficult to mention every friend and family members' name but sincere thanks to **Mr. Jeeeshan Ali** and **Mr. Vishvendra Tiwari** for their support thorough my journey here.

Thanks to everyone who has helped me achieve this.

# TABLE OF CONTENTS

# LIST OF FIGURES

# LIST OF TABLES

# Chapter 1 : INTRODUCTION

## 1.1 General

The surface waves are damage more to both the surface and sub-surface long-span structures when compare with the body waves since they can generate large strain in the long-span structures in addition to the load reversals. Further, in the case of sub-surface long-span structures, developed strain during earthquake is only responsible factor for the damage. It is now accepted by the seismological community that Rayleigh waves with high frequency and high amplitude can generate in case of shallow earthquakes at epicentral zone Narayan and Kumar (2010). However, till date no emphasis is given worldwide to predict the Rayleigh wave characteristics in the epicentral zone of large earthquakes in the research domain as well as in the earthquake resistant designs of long-span structures. So, there is an urgent need of quantification of characteristics of Rayleigh waves in terms of epicentral distance and focal-depth.

Narayan and Kumar (2010) reported that the incident P-wave and SV-wave at the free surface in a homogeneous half-space can generate Rayleigh wave. Their study states that as the focal depth increase then decrease of both the frequency content and amplitude in the produced Rayleigh waves occur. According to Narayan and Kumar (2010), the maximum conversion of energy of the incident P- and SV-waves in to Rayleigh wave energy occurs for that constant value for which the focal depth is around 0.17 times the wavelength of Rayleigh wave for the incident *P*- waves and 0.9 in the case of *SV*-waves at the free surface.

However, due to the lack of computational memory, Narayan and Kumar (2010) used very shallow point source and a frequency bandwidth for Ricker wavelet 0-5 Hz only. Further, they were unable to simulate the response at very large epicentral distance to separate out the Rayleigh waves from the direct incident SV-wave. Narayan and Kumar (2010) also considered focal depth up to 30 km but used frequency band up to 0.7 Hz only. Because of used limited frequency bandwidth and non-proper separation of the Rayleigh wave from the direct incident SV-wave, the computed response of spectral amplitude of normalized response with the spectral amplitude of the source function (Ricker wavelet) become unstable in the low and high frequency range. So, Narayan and Kumar (2010) were unable to infer the exact proportion of focal depth to Rayleigh wave

wavelength corresponding to peak value as well as were unable to compute the % amount of energy of incident SV-wave changed in to the Rayleigh wave energy. Furthermore, they were unable to give the proper reasoning for the reduction of amplitude and frequency bandwidth of Rayleigh wave with an increase of focal depth.

In order to accomplish the above identified technical gaps, we have simulated the seismic record of a homogeneous half-space model with a sufficient bandwidth in the Gabor wavelet and Ricker wavelet as well as focal depth up to crustal earthquakes. To find out the effects of duration of STF and Poisson's ratio on the characteristics of the generated Rayleigh wave, the seismic record of homogeneous half-space model for different cut-off frequency in the Gabor wavelet, dominant frequency in the Ricker wavelet and Poisson's ratio are computed and analyzed and presented in this thesis.

## 1.2 Rayleigh Wave Characteristics

The propagation of Rayleigh wave was described by the Lord Rayleigh in 1985. It also explains a semi-infinite elastic half-space wave propagation along free surface. The particles are polarized to quiver in the vertical plane. The resulting particle motion can be stared as a combination of P and SV waves vibrations. The particle motion describes a retrograde ellipse in the direction perpendicular to the wave propagation with its major axis and wave propagation direction along the minor axis, if the direction of propagation to the right of viewer.

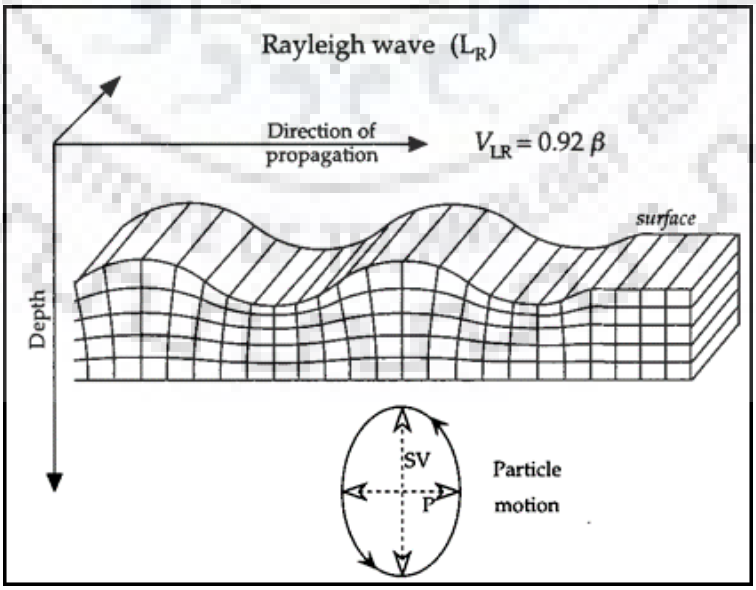


**Figure 1.1** Propagation of Rayleigh wave. ((Ewing et al. 1957))

Further, the movement of particles is not limited completely to the medium surface. when the Rayleigh wave passing below the free surface than Particles are also get affected. In a non-varying half space, the particle amplitude movement reduces exponentially with increase in depth. The surface wave and its penetration depth is characteristically taken at that particular depth where the amplitude is reduced to ($e^{-1}$) of its value at the free surface. The characteristics penetration depth is around $0.4\lambda$ for Rayleigh waves by wavelength $\lambda$.

### 1.2.1 Rayleigh Wave Generation in Epicentral Zone

The Rayleigh waves caused by earthquakes were once supposed to seem only at very large epicentral distances (several hundred km). It is now known, however, that they can be noteworthy at much shorter distance (a few tens of km). The lowest epicentral distance for the appearance of Rayleigh waves depend on the ratio of P-wave and SV- wave velocity of the homogeneous medium (Ewing et al. 1957). It can be the ratio of minimum epicentral distance '*R*' to corresponding focal depth '*h*'.

$$\frac{R}{h} = \frac{1}{\sqrt{\left(\frac{V_P}{V_R}\right)^2 - 1}} \tag{1.1}$$

Where $V_P$ and $V_R$ are velocities of P-wave and Rayleigh wave, respectively.

### 1.2.2 Rayleigh Wave Velocity in Homogeneous Medium

Virieux (1986) suggested an approximate solution for velocity of the Rayleigh wave in the homogeneous medium.

$$k = \frac{0.87 + 1.12\nu}{1 + \nu} \tag{1.2}$$

where $k = \frac{V_R}{V_S}$ and $\nu$ is Poisson's ratio

$$\frac{V_S}{V_p} = \sqrt{\frac{1 - 2\nu}{2(1 - \nu)}} \tag{1.3}$$

It is obvious that the difference between shear wave velocity and Rayleigh wave velocity is very less, being the latter slightly smaller than the former. In particular, the range of variation of the Rayleigh wave velocity depends on the Poisson's ratio.

$$0.87 < \frac{V_R}{V_S} < 0.96 \tag{1.4}$$

## 1.3 Rayleigh Wave Generation

Rayleigh waves are generated in nature in both layered and homogeneous medium and following are the mechanisms for explanation of their generation.

### 1.3.1 Mode Conversion at Critical Distance

The incident SV-wave converts in to P-wave at the free surface due to mode conversion. The reflection angle of P-wave is more than that of incident angle for SV-wave. For a particular angle of incident (critical angle), the angle of reflection becomes 90 degree for the P-wave. Such P-wave is known as evanescence P-wave, which travels along the free surface. The corresponding distance is known as critical distance. Just at/after the critical distance there is favorable condition for the coupling of P-wave with the reflected SV-wave to generate Rayleigh wave by Narayan and Kumar (2010).

### 1.3.2 Trapping in Crustal Mass

The reflected SV- and SH-waves from the free surface and a discontinuity in the earth interior (say Moho) reflection with angle larger than critical angle is trapped in the crust. Now, the coupling of the reflected waves from the top of Moho and the free surface is responsible for the surface wave generation. The trapping of SV- and SH- waves in the crust is accountable for the generation of Rayleigh and Love waves, respectively.

### 1.3.3 Lateral Discontinuity (Basin Edge)

The moment of body waves along the edge of basin and its angle of reflection development from top and bottom of the basin larger than the critical angle is accountable for the trapping of body waves in the basin and in conclusion the generation of surface waves. Bard and Bouchon (1980), Narayan (2005).

# Chapter 2 : FINITE DIFFERENCE ALGORITUM FOR SIMULATION OF SEISMIC WAVE PROPAGATION

## 2.1 General

Staggered grid finite difference method by Madariaga (1976) is most beneficial method to simulate ground motion. The aptness of finite difference depends on the model edges absorbing boundary condition and free surface as well. the implementation of absorbing boundary condition on the model edges effects very much accuracy of finite difference method and the free surface boundary condition on the free surface. The Levander (1988) initially used stress imaging phenomenon in his P-SV wave fourth order spatially précised staggered grid FD scheme. Body wave acquired 5 to 6 grid point pre shorted wavelength in order to avoid dispersion of Rayleigh waves.

### 2.1.1 FD Approximation of P-SV Wave Equation

A forth-order accurate P-SV wave viscoelastic FD programs has been used to simulate the seismic responses of the considered various models Narayan and Kumar (2014). In Figure 2.1 shows the staggered grid technique, at the nodes the component of normal stress and Lame's parameters are defined and at the center of the grid the component of shear stress and the modulus of rigidity are defined. Density of media and particle velocity are defined at the nodes and elastic coefficients and an-elastic functions are defined at the equidistance from the two adjacent grid points.

The operative value of density of media defined at the middle of two contiguous grid points have been attained using an arithmetic mean (Moczo et al. 2002).

$$\rho_{i+\frac{1}{2},I} = \frac{\rho_{i+1,I} + \rho_{i,I}}{2} \tag{2.1}$$

$$\rho_{i,I+\frac{1}{2}} = \frac{\rho_{i,I+1} + \rho_{i,I}}{2} \tag{2.2}$$

The operative value of the modulus of rigidity, defined at the midpoint of grid has been attained using a harmonic mean (Moczo et al. 2002).

$$\mu_{i+\frac{1}{2},I+\frac{1}{2}} = \left[\frac{1}{4}\left(\frac{1}{\mu_{i,I}} + \frac{1}{\mu_{i+1,I}} + \frac{1}{\mu_{i,I+1}} + \frac{1}{\mu_{i+1,I+1}}\right)\right]^{-1} \tag{2.3}$$

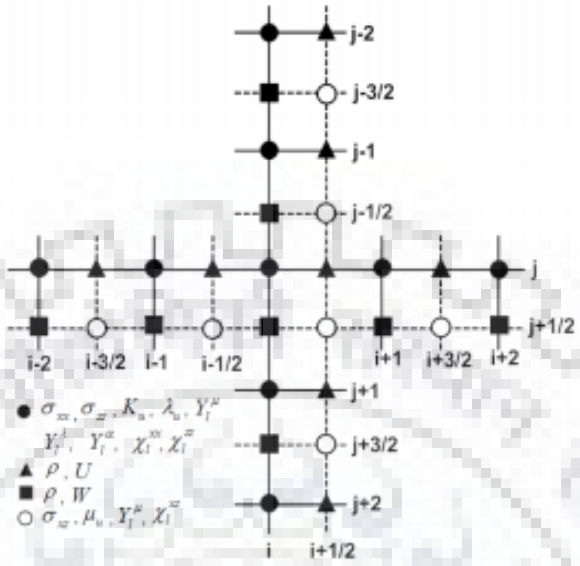


**Figure 2.1** P-SV wave model of staggered grid with fourth order spatial accuracy. Narayan and Kumar (2014)

### 2.1.2 Variable Grid Size

Uninterrupted grid with the variable grid size as proposed by Miyatake (1980) is used for the reduction of the computational time and memory. During the discretization of the model with variable grid size is continuous and discontinuous grid mesh may be used. Discontinuous grid size used only up to 3 grid size ratio. Larger grid size is used in the absorbing boundary zone to make the boundary condition more efficient.

### 2.1.3 Discretization of Model

The FD solution is a discrete estimate of a true solution. The exact velocities in the medium in grid is commonly vary from the time and group velocities. Grid dispersion is a very significant. On the propagation of the wave this effect become accumulative, as the distance travel is much, then greater the influence of the difference among the exact velocity and grid. The spatial sample ratio $s=\Delta x/\lambda$ depend on, the grid velocities where $\lambda$ is the wavelength that is to be propagated in the grid. The wavelength $\lambda$ in instruction to evade grid dispersion of the phase velocity and group velocities for wavelength $\lambda$ in fourth order approximation. In this study, we take minimum wavelength $\lambda_{min}$ is equivalent to the 6 grids spacing of sample.

$$\lambda_{\min} = 6\Delta x \tag{2.4}$$

### 2.1.4 Stability

The stability condition for this (2,4) P-SV wave FD approximation with variable grid size was got based on various iterative numerical trials. It depends on the time step and least grid size. The higher limit of time step for least grid size is evaluated on the basis of the stability condition.

A stability condition by Moczo et al. (2000).especially for fourth order spatial accuracy in the homogeneous medium for the P- and S- wave velocity. In the following equation there is $V_{max}$ is the maximum velocity in the homogeneous half space media. The minimum of the size considers in both the direction.at a particular node.

$$\frac{V_{\max}\Delta t}{\min.(\Delta x or \Delta z)} = \frac{6}{7\sqrt{2}} \tag{2.5}$$

### 2.1.5 Soil Amplification

The velocity of seismic wave is faster in hard rock as compare to the soft soil. When a wave enters from a high velocity zone to low velocity zone, it has to increase her amplitude to carry her energy. The fundamental resonance frequency of a sediment layer can be computed using the simple relation.

$$F_0 = \frac{V_S}{4H} \tag{2.6}$$

Where H is the thickness of the soil layer over the rock and Vs represent S-wave velocity in soil layer which overlay the rock with thickness H.

In order to authenticate the accuracy of the used finite difference program by Narayan and Kumar (2014) as well as to make sure that the required input parameters for the program are accurately computed, the seismic response of soil layer is computed. The rheological parameters for the soil layer and the rock are given in table 2.1.

**Table 2.1** Rheological parameters for the different layers of media.

| Medium | Vs(m/s) | Density (kg/m$^3$) | Quality factor | Thickness |
|---|---|---|---|---|
| Rock | 2000 | 2600 | 200 | ----- |
| Soil | 300 | 2000 | 30 | 39.0 m |

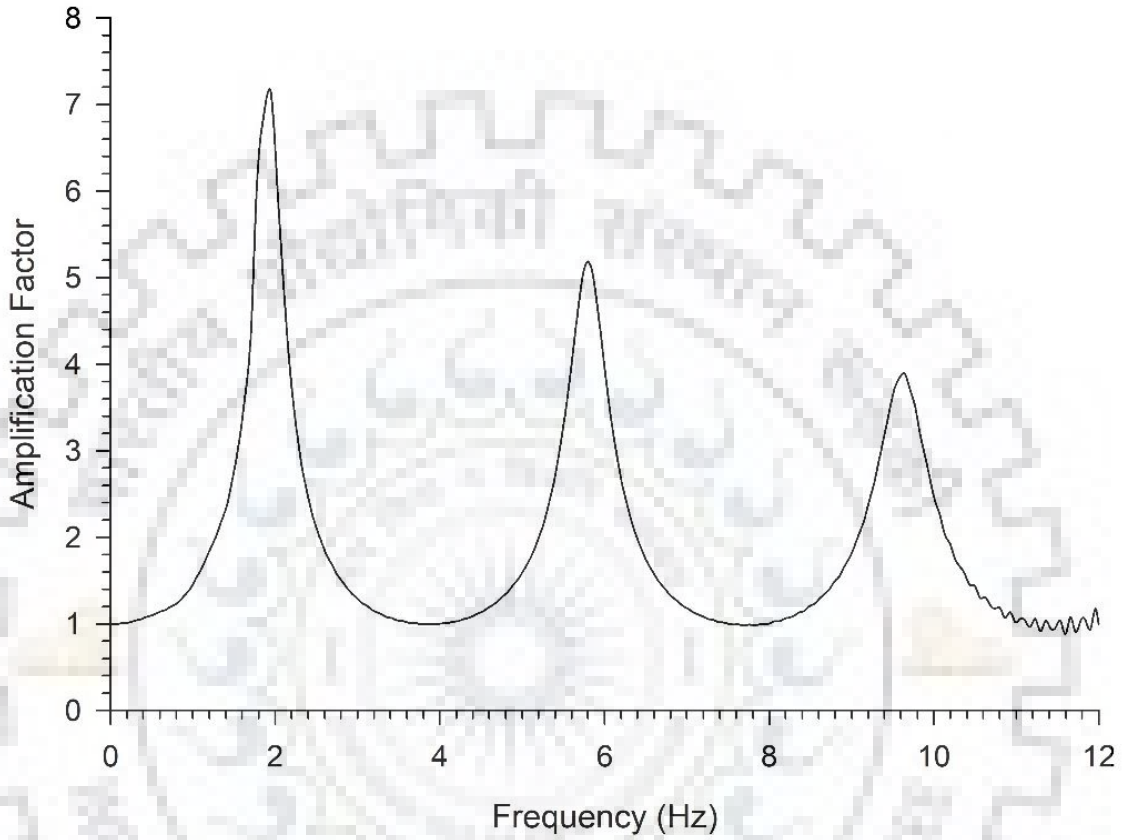


**Figure 2.2** Spectral amplification factors due to the soil effect

Figure 2.2 shows the computed soil amplification using the ratio of spectra of S-wave response of model for with soil layer of thickness H over the rock and only homogeneous rock layer in the model. Figure 2.2 clearly shows the amplification is 7.2 corresponding to the fundamental frequency of 2 Hz. The maximum amplification at the fundamental frequency can be computed by the following empirical relation.

$$A_0 = \frac{1}{\frac{1}{I.C.} + 0.5\xi\pi} \tag{2.7}$$

Where IC is impedance contrast, the empirically obtained amplification at fundamental frequency is 7.12 which is also same as the numerical analysis. This excellent match of

the computed fundamental frequency and corresponding amplification with those obtained empirically validate the accuracy of finite difference program as well as the procedure for the computation of an elastic coefficients and unrelaxed moduli, which are required as an input parameter.

## 2.2 Boundary Condition

### 2.2.1 Free Surface Boundary Condition

Free-surface boundary condition is the most important one factor to controlling the precision of elastic wave modeling technique. Free surface boundary condition can be attained using any of the stress imaging technique given by, Levander (1988), Gottschammer and Olsen (2001), Graves (1996); or the vacuum formulation by Boore (1972), Zahradník et al. (1993); Oprsal and Zahradnik (2002). In the vacuum formation, the values of elastic parameters are set to zero and density is reduced slightly above the free surface. This method is mostly used because it can be implemented with the same finite difference equation as used in the interior of the model.

### 2.2.2 Absorbing Boundary Condition

Because of the limited accessible computational computer memory, the numerical models have a certain fixed dimension. The waves travelling through the grid of the model are reflected back from the model edges, known as edge reflections. To evade these edge reflections, non-reflecting boundaries or absorbing boundary conditions are applied along the edge of the model. The boundary condition by Clayton and Engquist (1977) and absorbing boundary condition by Israeli and Orszag (1981) which is similar to the sponge is implemented on the half space model faces up to 800 grids from all the edges, to avoid the problem of the edge-reflections.

## 2.3 Source Implementation

### 2.3.1 Gabor Wavelet

A plane horizontal SV-wave front is produced in the FD numerical grid at some depth using point sources. A particular point source was produced using shear stress component $\sigma_{xz}$ in the form of Gabor wavelet. The following mathematical equation represents the Gabor wavelet.

$$S(t) = Exp(-\alpha)\cos(\omega_p(t - t_s) + \varphi) \tag{2.8}$$

Where $\alpha = \left(\frac{\omega_P(t-ts)}{\gamma}\right)^2$, $f_p$ is principal frequency, γ regulates the oscillatory character, $t_S$ regulates the duration (duration = 2 second) and ϕ is phase shift the created. The frequency content in the Gabor wavelet is 0 - 15.0 Hz. In this model Gabor wavelet used for the purpose of the study has $f_p$= 2 Hz, $t_S$ = 0.0025 s, γ=1.5 and ϕ=0.

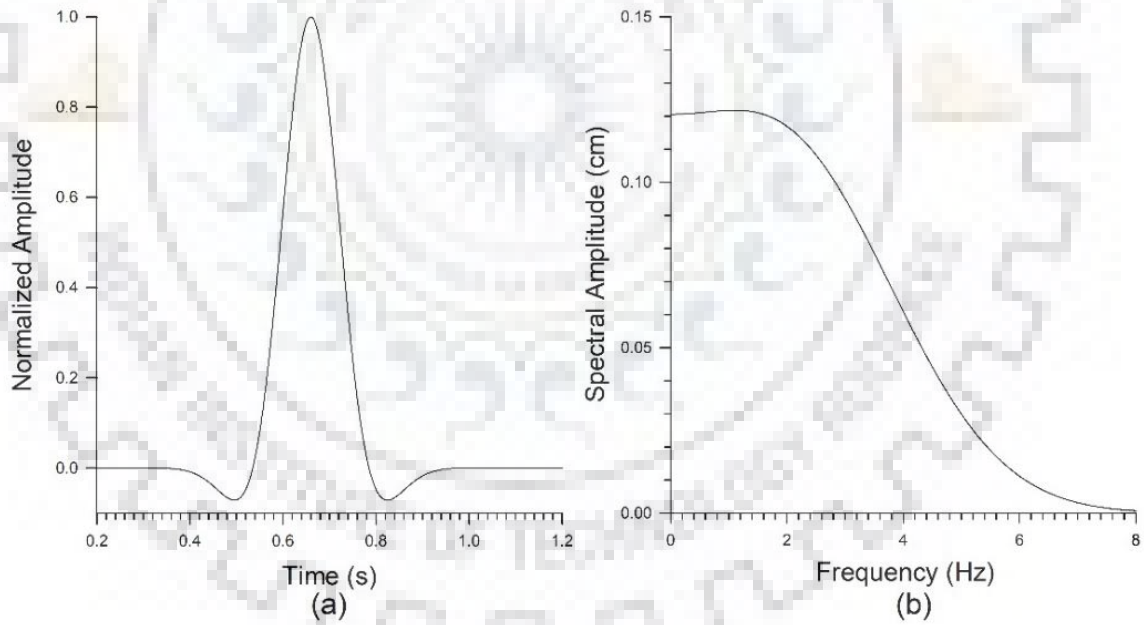


**Figure 2.3** Gabor wavelet and its spectra at 2.0 Hz cut-off frequency

The important property of the Gabor wavelet is that it minimizes the product of its standard deviation in the time and frequency domain. Gabor wavelet is used as transformation with either continuous or discrete input signal

### 2.3.2 Ricker Wavelet

A double couple point earthquake source based on the moment tensor source design may be applied into the computational grid using either stress component Coutant et al. (1995); Pitarka (1999); Narayan (2001) or velocity component. We have used the simply stress component in the form of Ricker wavelet, in the past, seismic simulation was also carried out using explosive source which is dominated by compressional wave. Virieux (1986)

The Ricker wavelet is created with the support of second derivatives of the convolution of a Gaussian function (H) and a polynomial window (G).

$$H = \exp\left[-\alpha(T - T_0)^2\right] \tag{2.9}$$

$$G = \left[1-\left(\tau - 1\right)^2\right]^3 \tag{2.10}$$

Where $\alpha = (\pi.F_0)^2$, $F_0$ is the cut-off frequency, $\tau = T/T_0$, time of wavelet represented by T and $T_0$ is time period. in the. Figure 2.3 shows the using 2 Hz dominant frequency STF for the generation of Ricker wavelet and its spectra with and upper cut-off frequency 6.0 Hz.

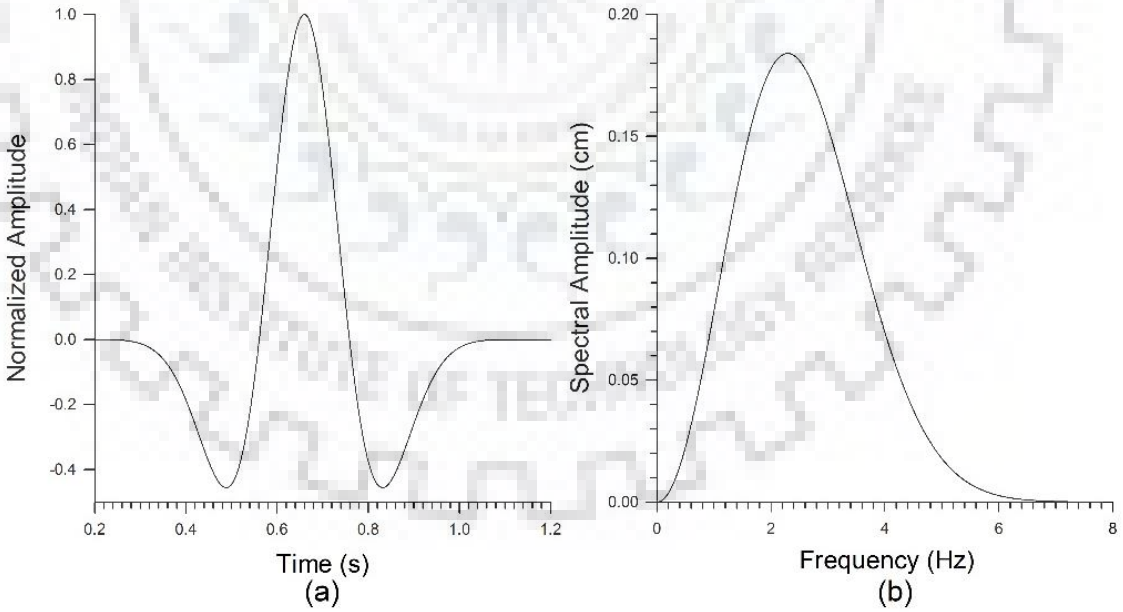


**Figure 2.4** (a) Ricker wavelet as source time function (b) spectral amplitude versus frequency

# Chapter 3 : RAYLEIGH WAVE GENERATION IN HOMOGENEOUS MEDIUM USING GABOR WAVELET AS SOURCE TIME FUNCTION

## 3.1 General

Narayan and Kumar (2010) reported that the incident P-wave and SV-wave at the free surface in a homogeneous half-space can produce Rayleigh wave. Their study state that as increases in the focal depth than the reduction in the amplitude and frequency content in the generated Rayleigh waves. According to Narayan and Kumar (2010), the maximum conversion of energy of the incident P and SV waves in to Rayleigh wave energy happens when the focal depth of the point source earthquake is nearly equal to the constant value 0.17 times the wavelength of Rayleigh wave and 0.9 in the case of incident *P*- and *SV*-waves at the free surface, respectively.

However, due to the deficiency of computational memory, Narayan and Kumar (2010) analyze very shallow point source and a frequency bandwidth for Ricker wavelet 0-5.0 Hz only. Further, they were unable to simulate the retort at very large epicentral distance to separate the Rayleigh waves from the direct incident SV-wave. Narayan and Kumar (2010) also considered focal depth up to 30 km but used frequency band up to 0.7 Hz only. Because of used inadequate frequency bandwidth and non-proper separation of the Rayleigh wave from the direct incident SV-wave, the calculated ratio of spectra of normalized response with the spectra of the STF (Ricker wavelet) become unstable in the low and high frequency ranges. So, Narayan and Kumar (2010) were unable to infer the exact proportion of focal depth to Rayleigh wave wavelength corresponding to peak value as well as were unable to compute the % amount of energy of incident SV-wave converted in to the energy of Rayleigh wave at the critical distance. Furthermore, they were unable to give the proper reasoning for the decrease of amplitude and frequency bandwidth of Rayleigh wave with an increase of focal depth.

In order to accomplish the above identified technical gaps, we have simulated the seismic record of a homogeneous half-space model with a sufficient bandwidth in the Gabor wavelet as well as focal depth up to crustal earthquakes. In order to analyze the effects of duration of STF and Poisson's ratio on the characteristics of generated Rayleigh

wave, the seismic record of homogeneous half-space model for different cut-off frequency in the Gabor wavelet and Poisson's ratio are computed and analyzed and presented in this chapter.

## 3.2 Rayleigh Wave Generation in Homogeneous Half-Space

To study the Rayleigh wave generation mechanism in homogeneous half-space as well as to study the effects of focal depth on the characteristics of the generated Rayleigh waves, the P-SV wave records of a homogeneous half-space model using a point source at different focal depths have been computed at different epicentral distance and dominated with the SV-wave. We have simulated the responses using the FD program formed by Narayan and Kumar (2014) for the viscoelastic P-SV wave propagation. Shear stress component $\sigma_{xz}$ is used for the production of SV-wave at the focus in the form of a wavelet i.e. Gabor wavelet (Source time function) with dominant frequency 2.0 Hz (with the considerable frequency bandwidth 0.02 Hz – 8 Hz).

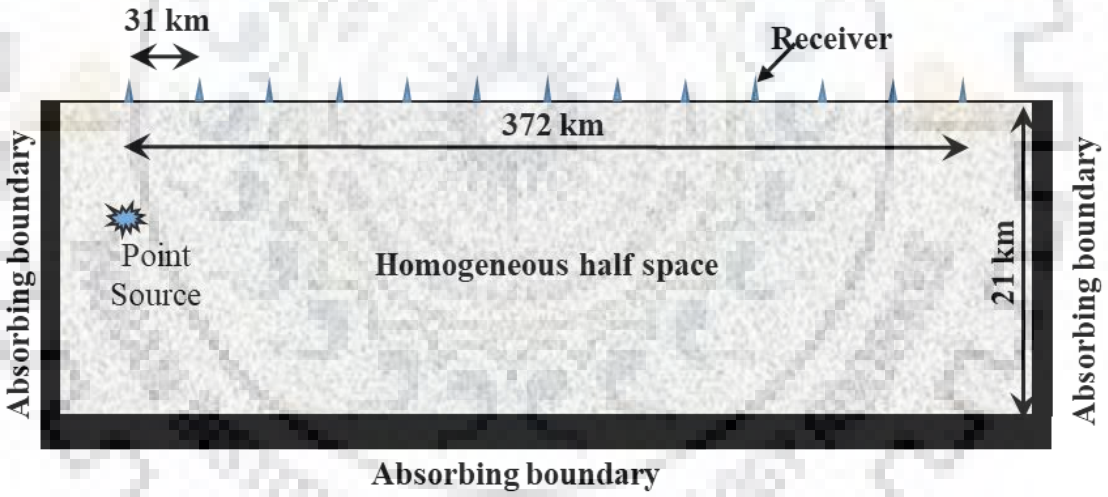


**Figure 3.1** Point source location in in homogeneous half-space model and recording array at the free surface

The homogeneous half-space model was discretizing with the variable size of grid. The size of grids in computational domain was taken as 25 meter in X-direction as the horizontal direction and along the depth of media up to depth of 21km it was 25 meter subsequently 60 meter. The time step is taken 0.0025 second to fulfill the stability condition. The horizontal and vertical components of seismic responses were figured at 13 equidistance (31 km apart) receiver points. The first receiver was kept at the epicenter and the last one was kept at an epicentral distance 372 km.

**Table 3.1** The rheological parameters of the homogeneous half-space model

| $V_P$ (m/s) | $V_S$ (m/s) | $V_R$ (m/s) | Density (kg/m$^3$) | $Q_P$ | $Q_S$ | Poisson's ratio |
|---|---|---|---|---|---|---|
| 5200 | 3000.00 | 2767.00 | 2800 | 520.0 | 300.0 | 0.25 |

### 3.2.1 Time-Domain Responses

The estimation of characteristics of Rayleigh waves in the epicentral zone of shallow earthquakes is a challenging job because of mixing of the Rayleigh waves with the SV-wave trains. Both the waves are recorded on all the three components and with more or less similar frequency bandwidth. Even though, frequency content in the Rayleigh wave is less, but, it is merged with the SV-waves. Finally, there is single parameter, the velocity difference between the Rayleigh and SV-waves, particularly in the case of layered earth. In order to separate out the Rayleigh waves from the SV-wave, we have to simulate the ground motion at larger epicentral distance, even more than 350 km. In the following sections, the effects of focal depth on the features of the generated Rayleigh wave are described.

#### 3.2.1.1 Focal Depth = 5.0 Km

In the Figure 3.2 the of seismic responses of the homogeneous half-space model at a 5.0 km focal depth of and *SV*-wave dominated source. The cut-off frequency used in the Gabor wavelet is 2.0 Hz. The seismic record at epicenter have signal only in the horizontal component and not in the vertical component (result not shown here). The seismic record at an epicenter of 31 km shows the direct P-wave, evanescence P-wave, SV-wave and the generated Rayleigh wave at the free surface in a sequential order in both the components. In comparison of the Rayleigh wave amplitude in vertical component is more than the horizontal component. Similar in case of SV-wave, this is the reason why detecting Rayleigh wave in the epicentral zone is very difficult. Further, the Rayleigh wave is mixed with the SV-wave. However, both the SV-wave and Rayleigh wave can be seeming since there is a single wavelet corresponding to both the waves. But, it will be very difficult in the case of earthquake rupture where there may be so many wavelets in both the waves. A split-up of Rayleigh wave clearly seems by increasing the epicentral distance. The analysis of figure 3.2 reveals that there is faster rate of decrease of amplitude of body waves as compared to the Rayleigh waves. The main reason behind this inference is the

divergence effects, although damping is occurring for both the body waves and the Rayleigh waves.

As far as divergence is concerned, it is occurring in the case of body waves since wave fronts are circular in nature, in the case of Rayleigh wave, it is not happening since wave front is linear (a cross section of cylindrical wave front with a fixed height) and wave is propagating in the XZ-plane. the vertical component of Rayleigh wave amplitude is around 1.5 times to that in the horizontal component. The Rayleigh wave separation with the SV-wave can be seen with an increase of epicentral distance. Even in this simple point source modeling, the required epicentral distance is 372 km to separate out the lower frequency Rayleigh wave from the SV-wave.

#### 3.2.1.2 Focal Depth = 6.0 Km

The horizontal (x) component and vertical (y) component of seismic record of the homogeneous half-space model by *SV*-wave dominated point source at focal depth 6.0 km is shown in figure 3.3. Again, the response at epicenter distance (at 0 km) have signal only in the horizontal component and not in the vertical component (result not shown here). The seismic record at an epicenter of 31 km clearly shows the direct P-wave, evanescence P-wave, SV-wave and the generated Rayleigh wave at the free surface in a sequential order in both the horizontal component and vertical component. The Rayleigh wave is mixed with the SV-wave. However, both the SV-wave and Rayleigh wave can be seen since there is a single wavelet corresponding to both the waves.

The analysis of figure 3.3 shows that there is faster rate of decrease of amplitude of body waves as compared to the Rayleigh waves, as was observed in the previous case. This is because of the divergence effects, while damping is occurring for both the body waves and the Rayleigh waves. A split-up of Rayleigh wave with the SV-wave can be seen with an increase of epicentral distance. Even in this simple point source earthquake modeling, the required epicentral distance is 372 km to separate out the low frequency Rayleigh wave from the SV-wave.

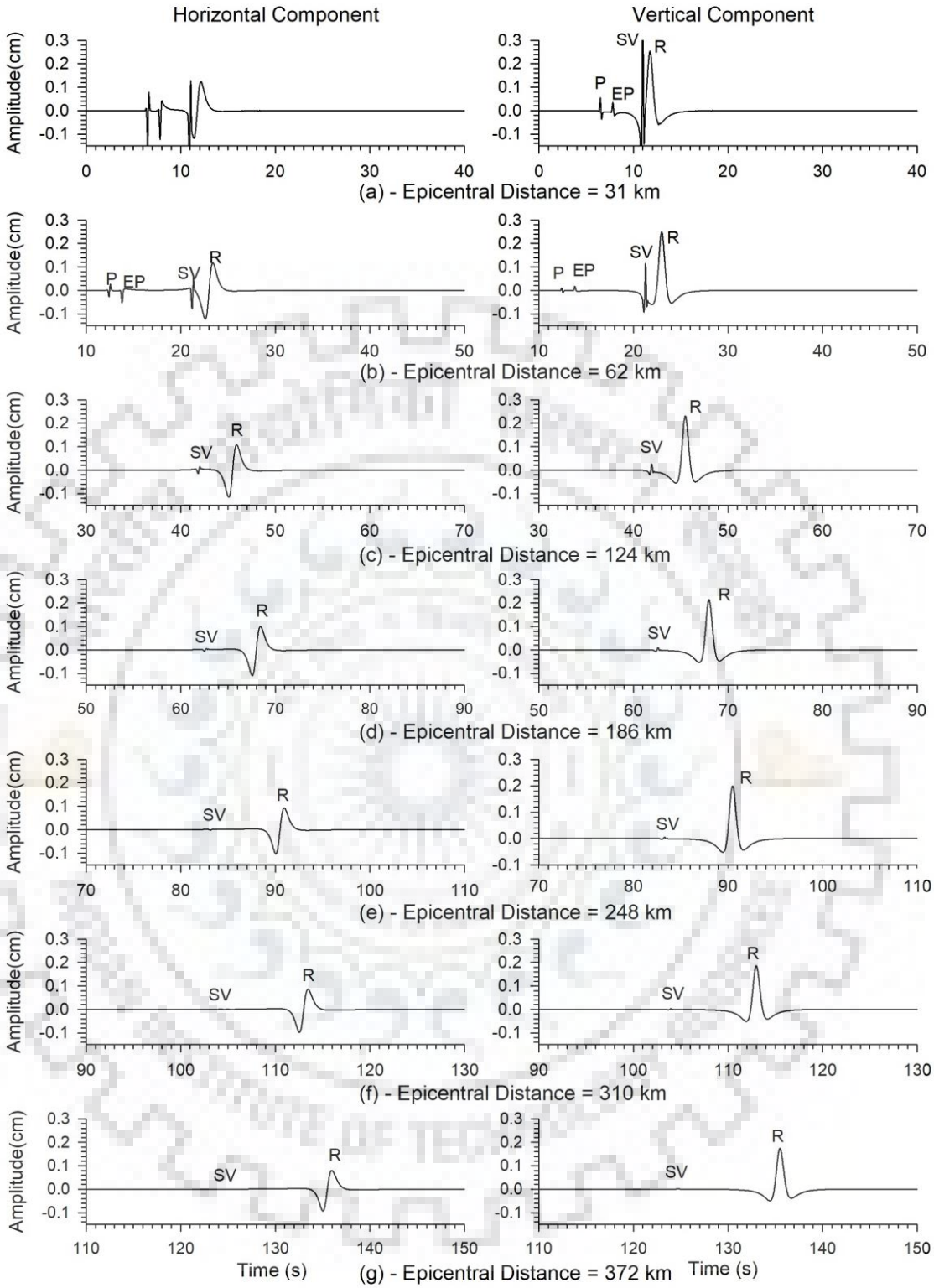


**Figure 3.2** The seismic record of homogeneous half-space model at different epicentral distances using a SV-wave dominated point source earthquake at a depth of 5.0 km (Gabor wave is used as STF)

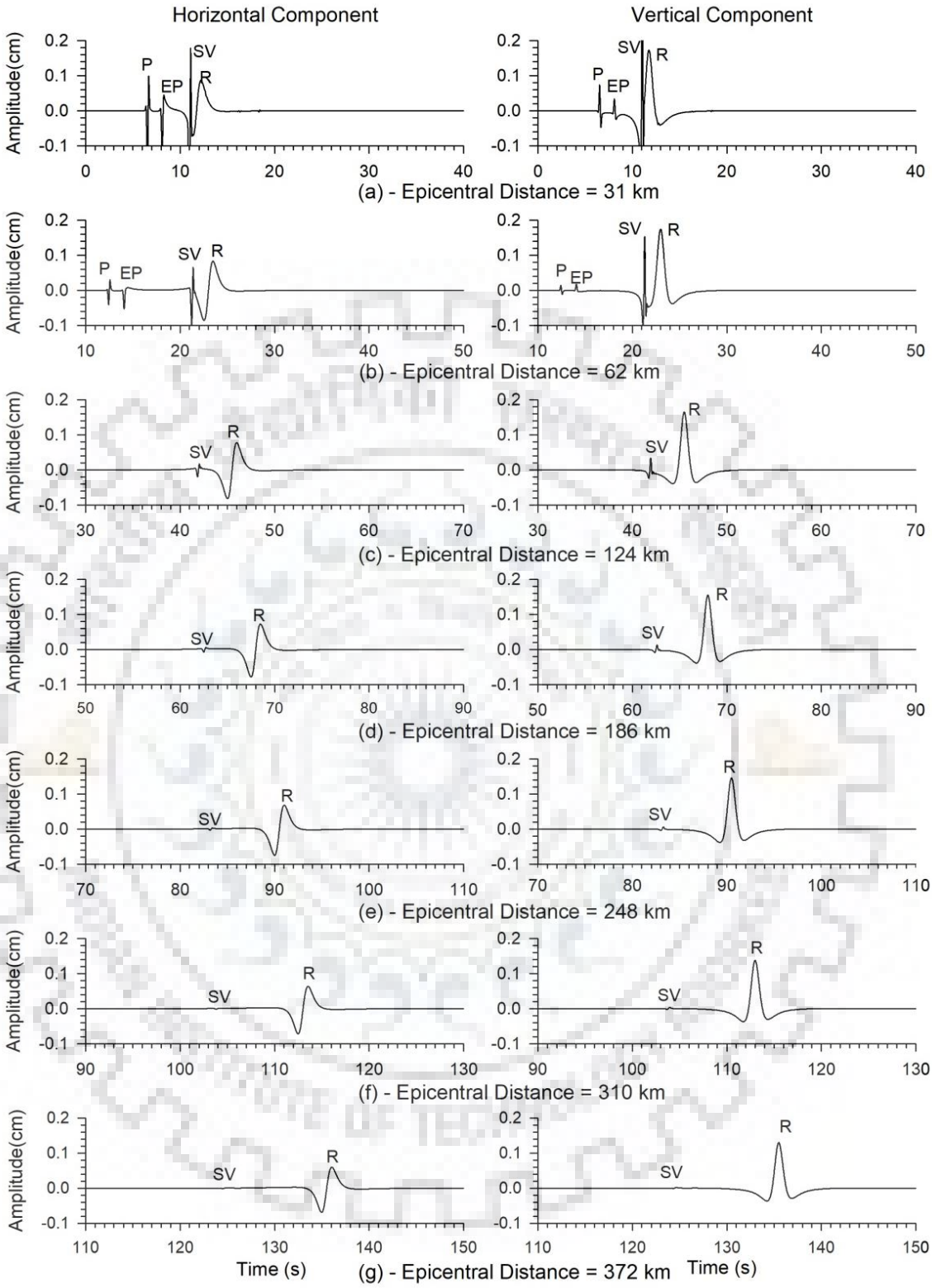


**Figure 3.3** The seismic record of homogeneous half-space model at different epicentral distances using a SV-wave dominated point source earthquake at a depth of 6.0 km (Gabor wave is used as STF)

Similarly, figures 3.4 to 3.9 show the horizontal component (left panels) and vertical component (right panels) of seismic record of homogeneous half-space model for following focal depths 7.5 km to 20.0 km (6 cases), respectively. In these cases, also, Rayleigh waves can be identified, even at an epicentral distance of 31 km, excluding when focal depth is more than 15 km, the amplitude of the direct incident SV-wave is too large as compared to the produced Rayleigh wave. Now, the analysis of figures 3.4-3.9 reflects that there is reduction in amplitude of Rayleigh wave as the focal depth increases. While, there is the amplitude of SV-wave decrease also due to the increase of hypo-central distance at the critical distance. Still, Rayleigh wave can be recognized after an epicentral distance of 124 km in the cases where focal depth is more than 15 km. But, the Rayleigh wave is not totally separated from the SV-wave.

As the focal depth increases then the duration of the wavelet of the Rayleigh wave increases. This may be due to the decrease of frequency content in the generated Rayleigh wave. However, in all the cases, the Rayleigh waves are well detached from the SV-wave only at epicentral distance of 372 km. One of the reasons for the required large epicentral distance to separate out the Rayleigh wave from the SV-wave may be the longer duration of Rayleigh wave wavelet in the case of deeper focal depths.

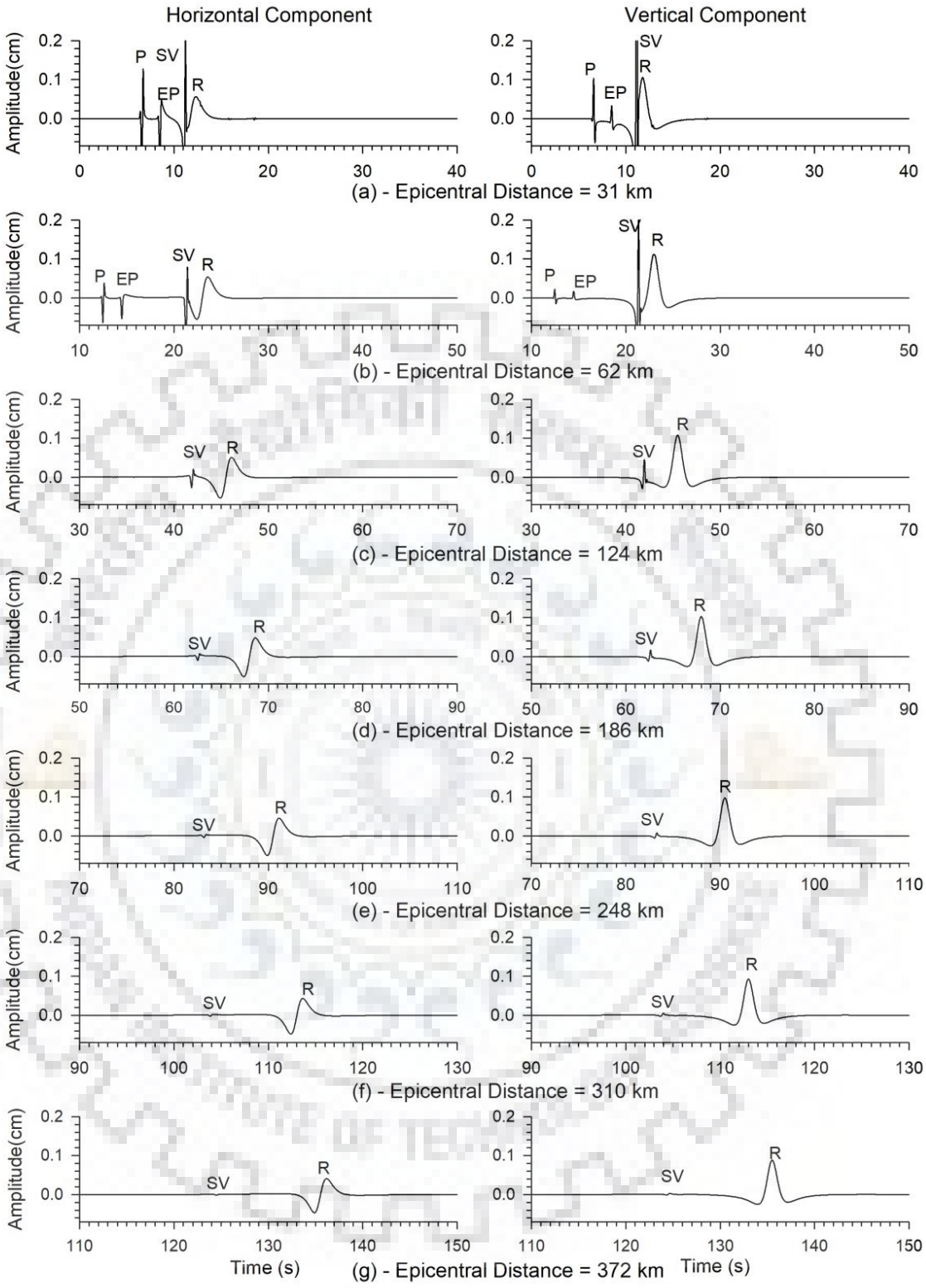


**Figure 3.4** The seismic record of homogeneous half-space model at different epicentral distances using a SV-wave dominated point source earthquake at a depth of 7.5 km (Gabor wave is used as STF)

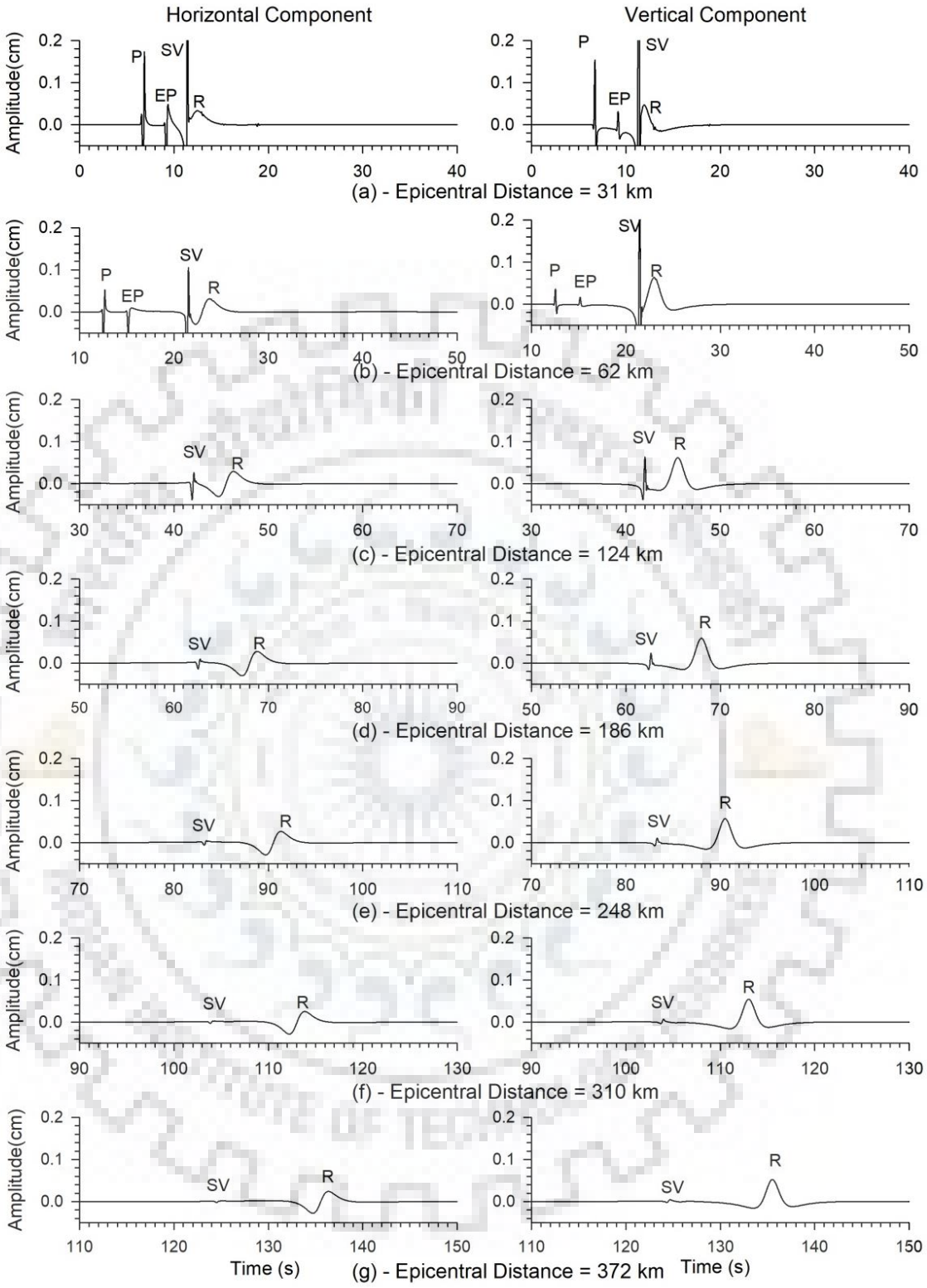


**Figure 3.5** The seismic record of homogeneous half-space model at different epicentral distances using a SV-wave dominated point source earthquake at a depth of 10.0 km (Gabor wave is used as STF)

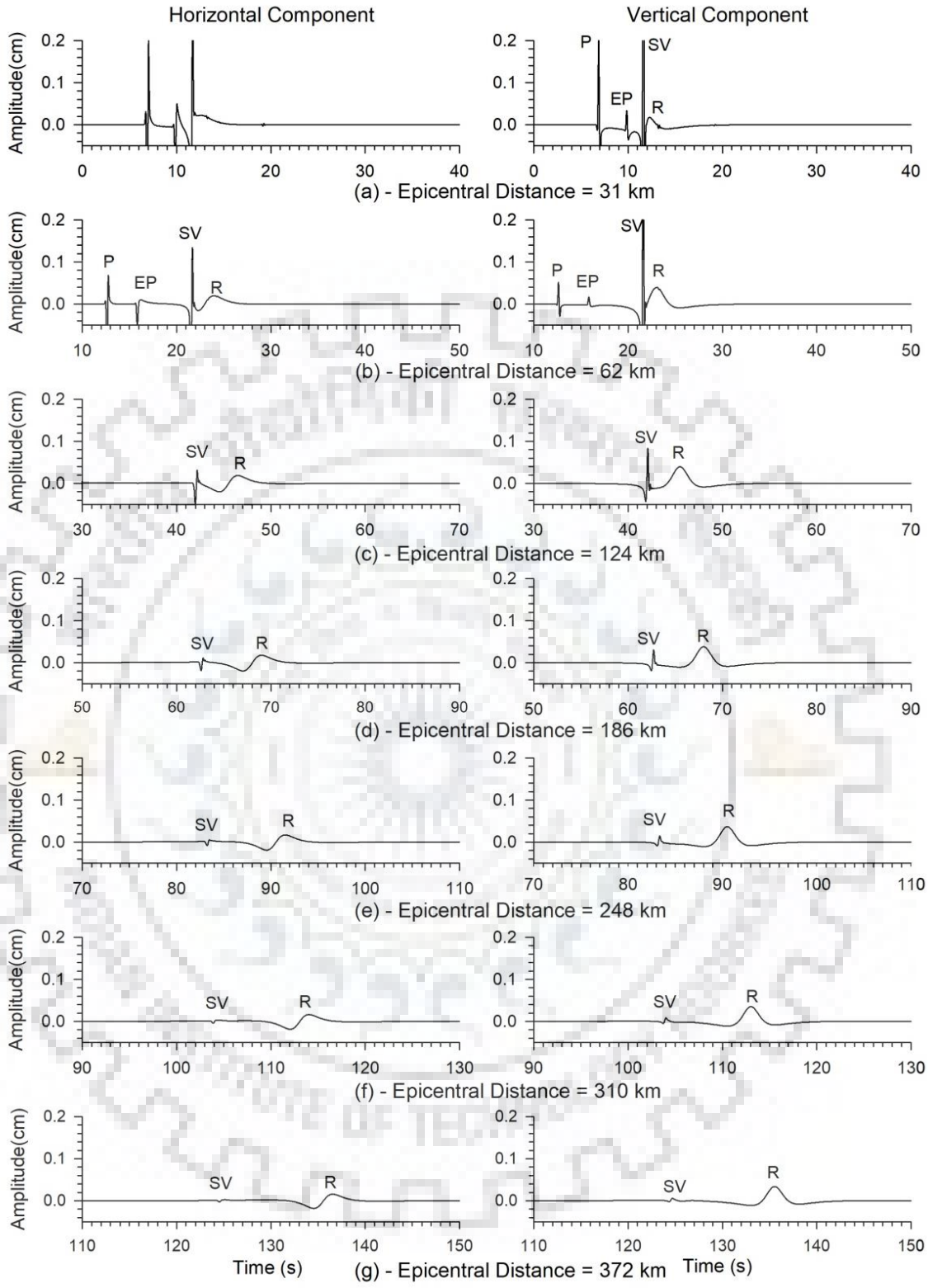


**Figure 3.6** The seismic record of homogeneous half-space model at different epicentral distances using a SV-wave dominated point source earthquake at a depth of 12.5 km (Gabor wave is used as STF)

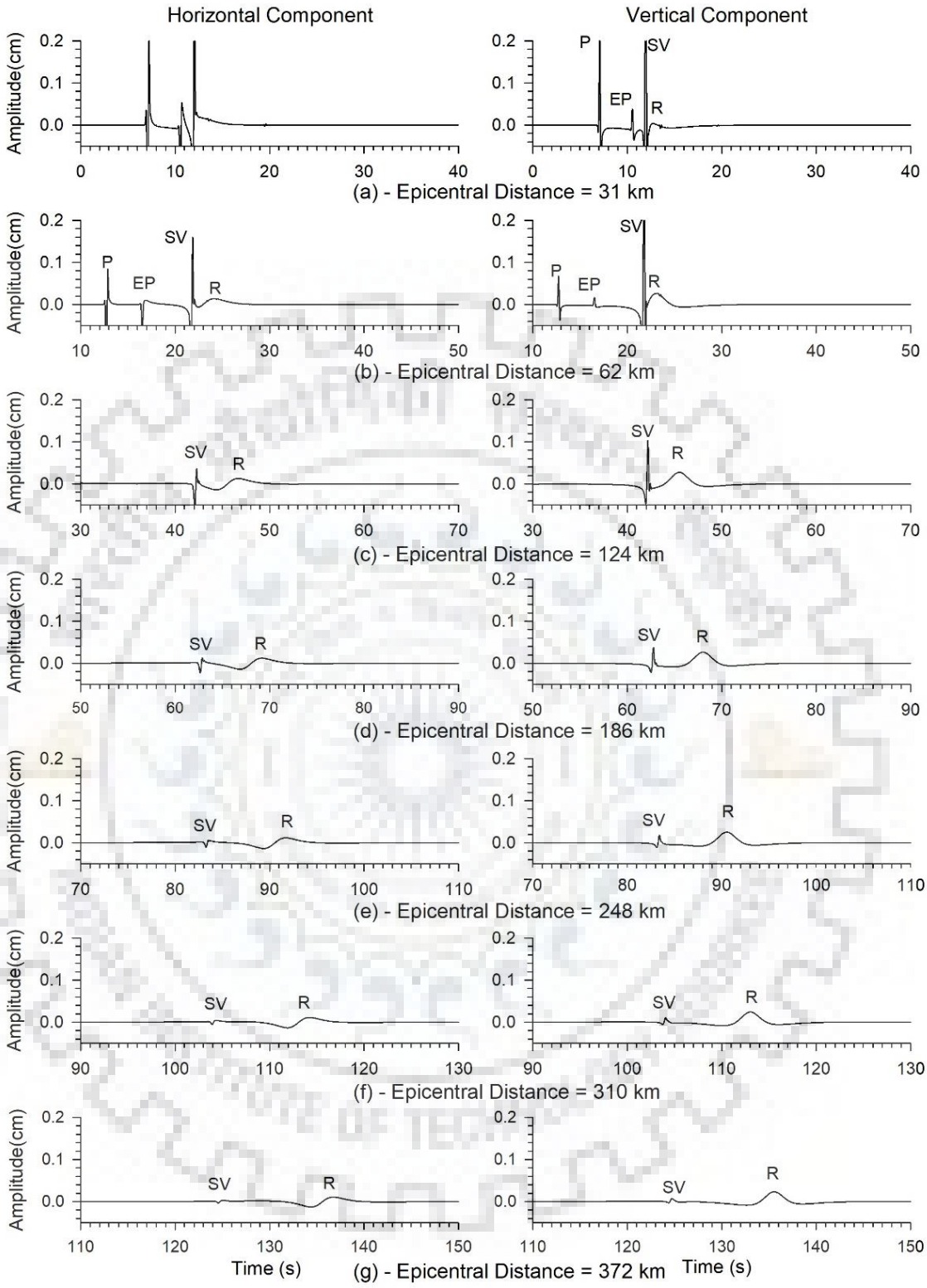


**Figure 3.7** The seismic record of homogeneous half-space model at different epicentral distances using a SV-wave dominated point source earthquake at a depth of 15 km (Gabor wave is used as STF)

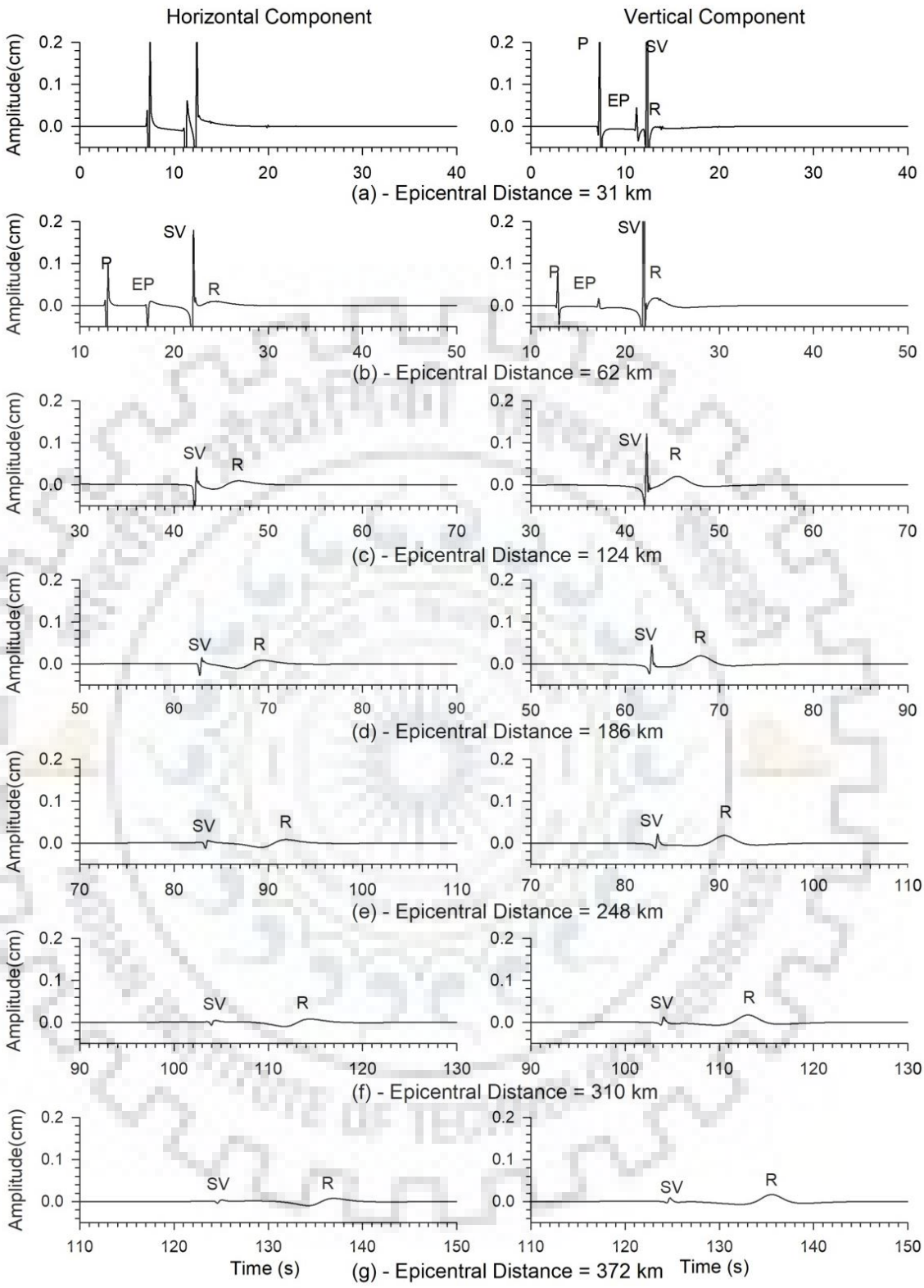


**Figure 3.8** The seismic record of homogeneous half-space model at different epicentral distances using a SV-wave dominated point source earthquake at a depth of 17.5 km (Gabor wave is used as STF)

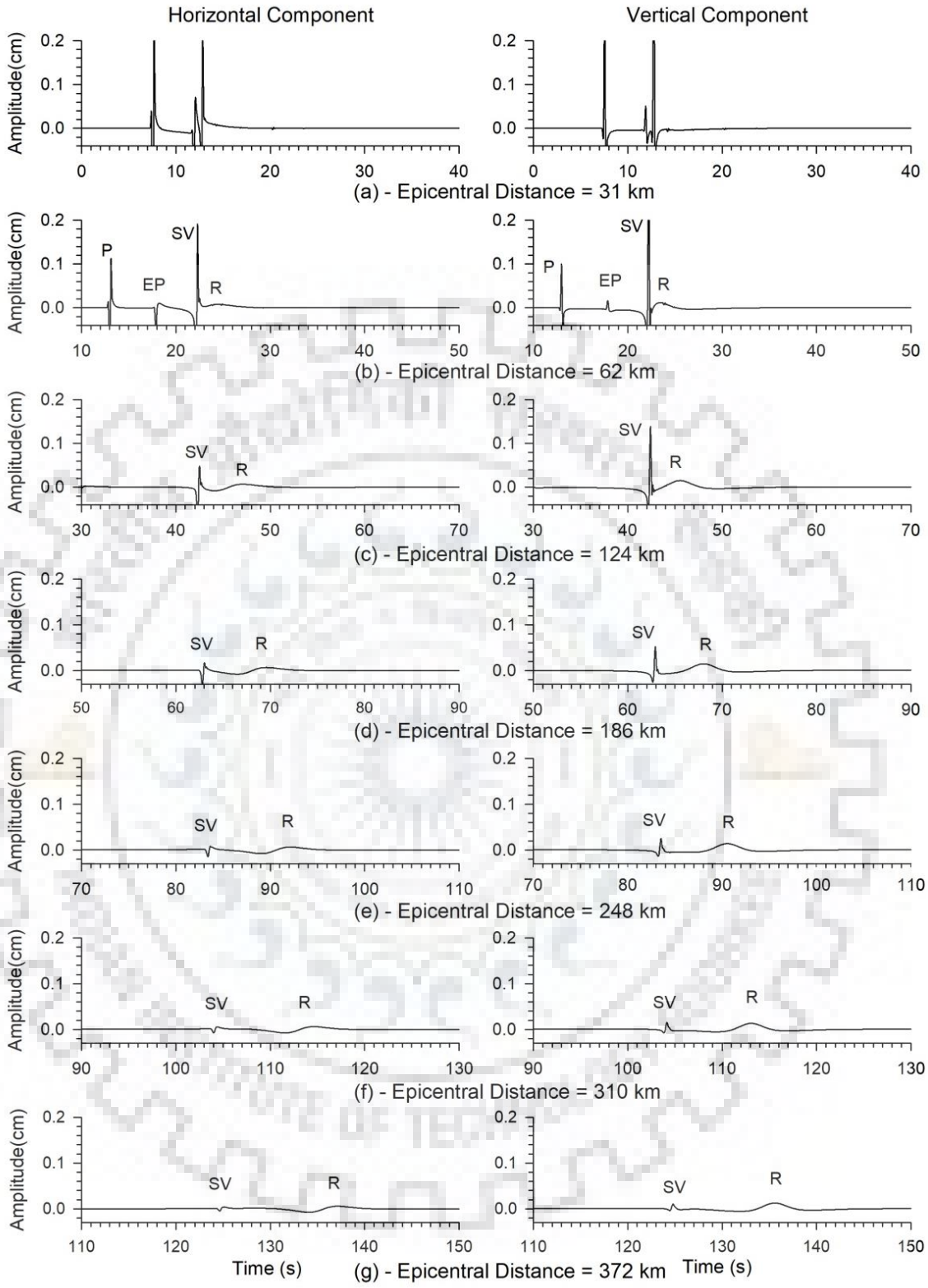


**Figure 3.9** The seismic record of homogeneous half-space model at different epicentral distances using a SV-wave dominated point source earthquake at a depth of 20.0 km (Gabor wave is used as STF)

### 3.2.2 Analysis of Simulated Results

#### 3.2.2.1 Effects of Curvature of Wave Front

There is generation of Rayleigh wave in all the cases of focal depths; however, as the focal depth rises than there is reduction of frequency and amplitude content in the Rayleigh wave. Now, question arise why there is amplitude of Rayleigh wave drops by a increase of focal depth. In all the cases, the rheological parameters, free surface properties and frequency content in the STF are same except the minor drop of amplitude of the incident SV-wave at the free surface due to the damping and divergence effects. However, the drop of amplitude of the Rayleigh wave is not in proportion to the drop of amplitude of the SV-wave. Further, there is reduction of frequency content in the generated Rayleigh wave also. So, the only accountable parameter for the reduction of the amplitude and frequency of generated Rayleigh wave may be the drop of curvature of the wave front of the incident SV-wave. So, the only responsible parameter for the drop of amplitude and frequency of the generated Rayleigh wave may be the drop in curvature of the wave front of the incident SV-wave.

#### 3.2.2.2 Location at Free Surface for the Rayleigh Wave Generation

Now, next question arises the location at which Rayleigh waves are being generated. The Rayleigh waves are generated due to the coupling of the P- and SV-waves at/after the critical distance. This is only possible at the free surface due to the mode translation of the SV-wave to P-wave and from the P-wave to SV-wave. There will no mode translation at the epicenter. Further, in the case of incident SV-wave, there will be no mode translation after the critical distance. Means, the location at the free surface for the generated of Rayleigh wave is between the epicenter and the critical distance. Now, again question arise, are there so many place between epicenter and the critical distance which can cause Rayleigh wave, since there is mode converted P-wave and a favorable place for coupling. But, the observed single wavelet of the generated Rayleigh wave and the matching of the wavelet shape corresponding to the vertical component with the STF (Gabor wavelet) depicts that there is only single point between epicenter and the critical distance which can cause Rayleigh wave. The observed phase difference between the horizontal and vertical components of Rayleigh wave is $90^0$, which is obvious in the case of homogeneous medium. So, finally, there is a single point i.e. the critical distance at which the mode converted P-wave starts travelling along the free surface and the coupling

with the reflected SV-wave is responsible of the generation of Rayleigh wave. The mode converted P-wave which stars travelling along the free surface is known as evanescence P-wave.

There will be an increase of critical distance from the epicenter with the increase of focal depth. The observed reduction of time departure between the evanescence P-wave and the Rayleigh wave at a particular epicenter distance (say 31 km) with the increase of focal depth as well as a single wavelet of the generated Rayleigh wave supports the generation of Rayleigh wave at the critical distance.

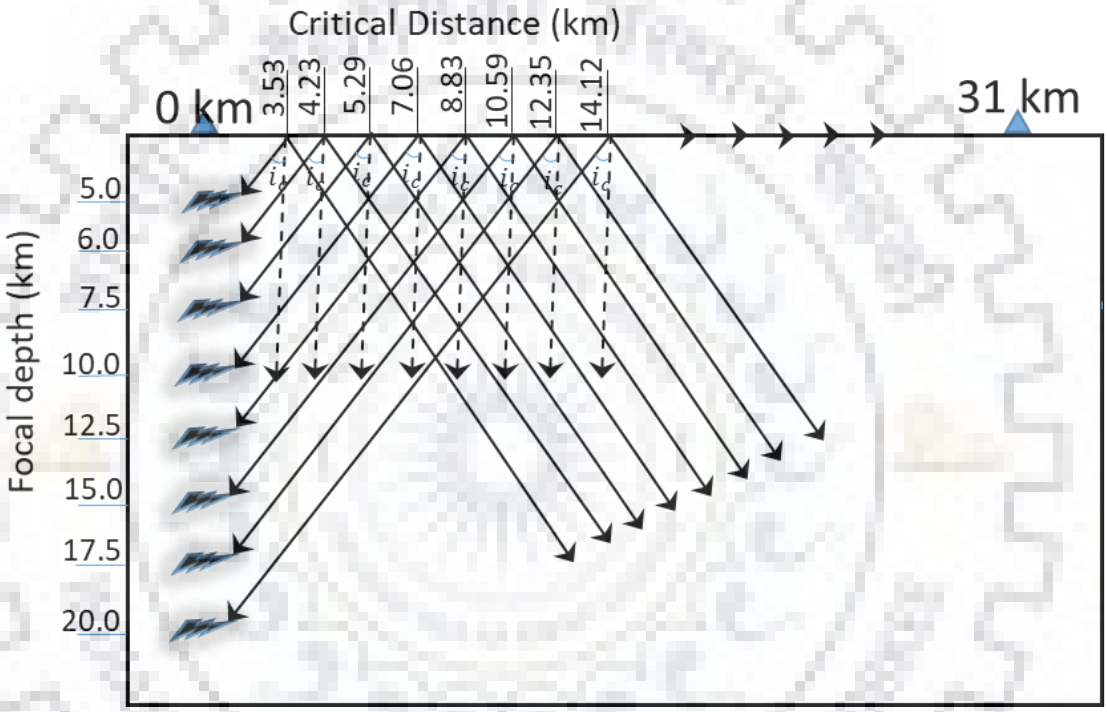


**Figure 3.10** Plot of the critical distance for different focal depth of the homogenous half space model

### 3.2.2.3 Spectral Analysis

The left and the right panels of figure 3.11a show the both components of the computed seismic record at an epicenter of 372 km for the different focal depths of point earthquake source. The analysis of figure 3.11a shows the drop of Rayleigh wave amplitude with increase of focal depth. Further, increase of the focal depth there is reduction of frequency content in the Gabor wavelet STF, which is reflected in the form of widening of the wavelet. In order to achieve the spectral amplitude of generated Rayleigh wave corresponding to the unit spectral amplitude of the incident SV-wave at the epicenter, the spectra of traces recorded at the epicenter of 372 km are normalized with the spectra of

the traces recorded at the epicenter. In figure 3.11b there is consideration of only Rayleigh wave part from the record of different focal depth at an epicenter of 372 km and plot the graph between the normalized spectral amplitude (normalized with the spectra of STF) and the frequency.

An analysis of figure 3.11b shows that the reduction of frequency bandwidth of the generated Rayleigh wave with an increase of focal depth of point source. Further, the peak normalized spectral amplitude and the frequency content where peak occurs is also reducing with increase in focal depth. Figure 3.12a clearly shows the almost exponential drop of peak frequency in horizontal and vertical component with an increase of focal depth. On an average, rise of spectral amplitude in lower frequency and drop in higher frequency with respect to the dominant frequency can be observed. To see whether there is a specific frequency corresponding to there is maximum translation energy of SV-wave in Rayleigh wave normalized spectral amplitude versus the $FD/\lambda$ ratio for different focal depths and shown in figure 3.11c (where FD is focal depth and $\lambda$ is the wavelength of the Rayleigh wave). The constant ratio of focal depth and wavelength of the Rayleigh wave was found for all the focal depth corresponding to their maximum normalized spectral amplitude occurs at the value of $FD/\lambda = 0.63$ and the remaining other ratio before and after the $FD/\lambda = 0.63$ there is exponential reduction of normalized amplitude of the Rayleigh wave. So, considering this point, we conclude that the maximum energy of the *SV*-wave converts into the energy of Rayleigh wave at the critical distance when focal depth is equal to 0.63 times to that of the wavelength of Rayleigh-wave.

Further, figure 3.12b depicts that the normalized spectral amplitude for focal depths where the peak of frequency is occurring. There is the horizontal and vertical component clearly so that the normalized amplitude of vertical component is 1.5 more than the horizontal component. The reduction of the normalized amplitude with increasing the focal depth. The reduction in normalized amplitude in both the component (horizontal and vertical) is almost exponential.

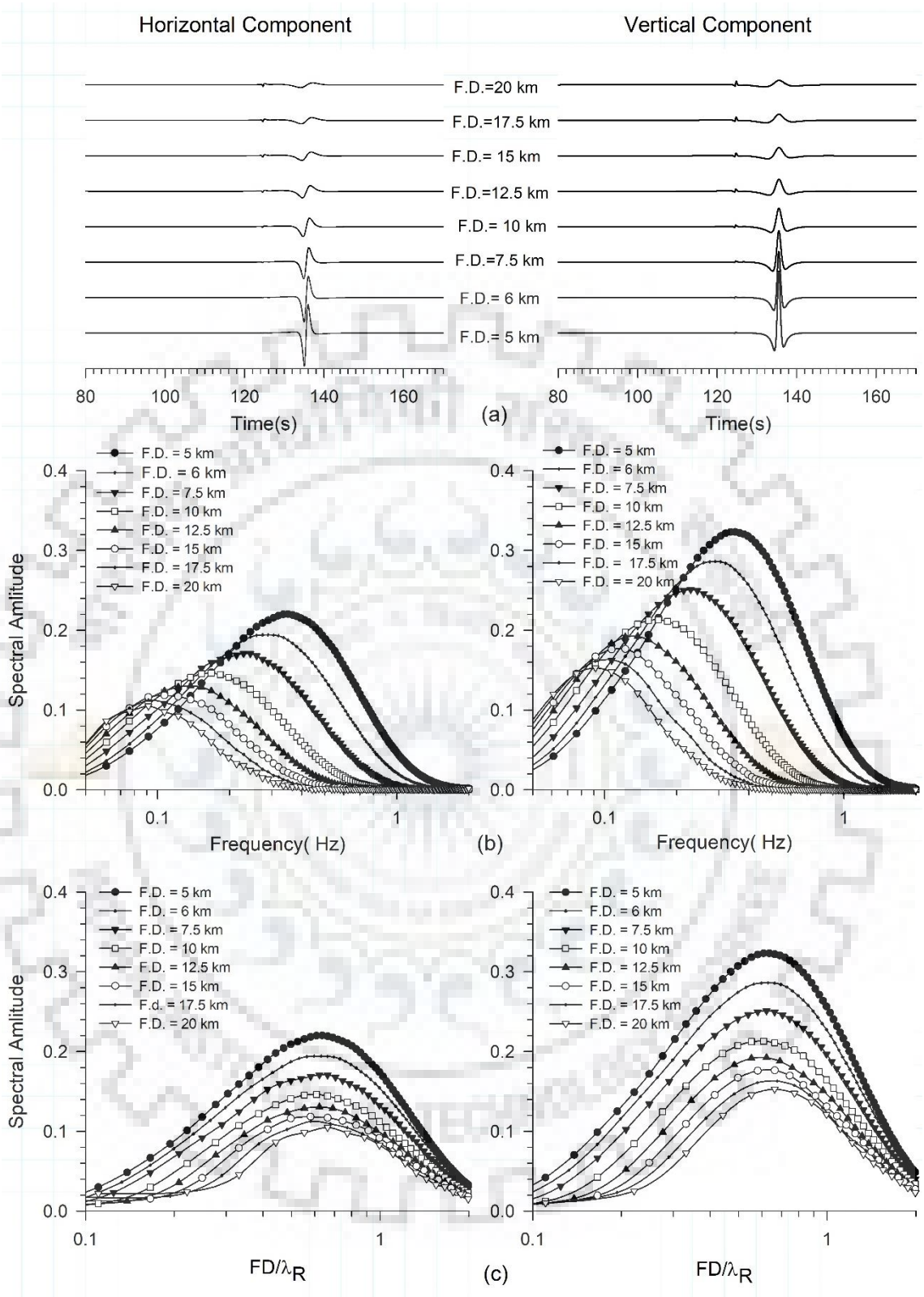


**Figure 3.11** (a) The seismic record for different focal depths at epicenter of 372 km (b) analysis of the spectra of only Rayleigh wave part at epicenter of 372 km for different focal depths (c) study of the spectral amplitude of only Rayleigh wave at epicenter of 372 km with the ratio of different focal depth to the Rayleigh wave wavelength

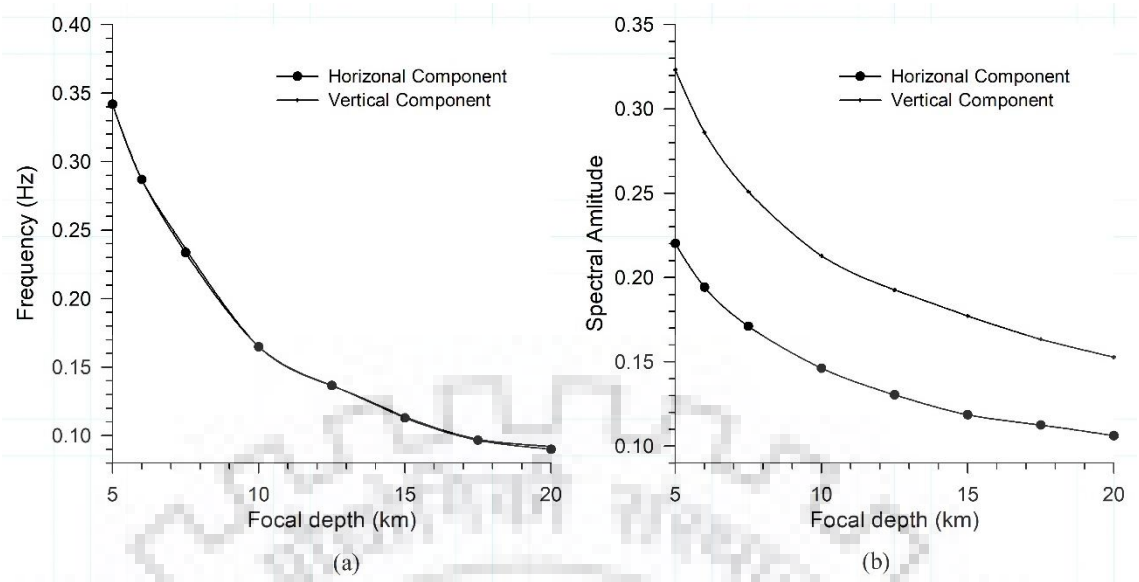


**Figure 3.12** (a) The peak frequency of horizontal and vertical component at epicentral distance of 372 km for different focal depths (b) The peak normalized spectral amplitude corresponding to their frequency for different focal depth (Gabor wave is used as STF)

To calculate the conversion of the energy of incident SV-wave at the critical distance also considering the divergence effect of focal depth at critical distance, which is the ratio of the shortest distance between hypocenter to critical distance with the focal depth. We can calculate it by the attention relationship of a seismic wave which depends on the frequency and damping parameter (quality factor). Where $\lambda$ is the wavelength of the Rayleigh wave, $r$ is the distance between critical distance to 372 km and $Q$ is the quality factor.

$$A = A_0 e^{\left(\frac{-\pi r}{Q\lambda}\right)} \tag{3.1}$$

Than after consideration of the above formula the energy conversion of the incident SV-wave at the critical distance in to the Rayleigh wave with the Gabor wavelet as a STF is calculated by adding the peak normalized amplitude of the both component. table 3.2 clearly show that the reduction of the converted energy of the incident SV-wave to Rayleigh wave at the critical distance with increase in the focal depth. The largest spectral amplitude of the prominent frequency of Rayleigh wave for unit amplitude of the incident SV-wave at the critical distance was obtained as 56% and 26% corresponding to focal depths 5 km and 20 km, respectively.

**Table 3.2** The variation of obtained prevailing frequency ($F_P$), amplitude in the horizontal ($H$) and vertical ($V$) components of Rayleigh wave of frequency $F_P$ at the critical distance with focal depth corresponding to the unit spectral amplitude of the incident SV-wave at the critical distance in the Gabor wavelet

| **Focal depth (km)** | **Critical distance (km)** | ***$F_P$* (Hz), amp. in *H*- & *V*- comp. of R-wave at *$F_P$* at critical distance (Gabor wavelet case)** | | | |
|---|---|---|---|---|---|
| | | **$F_P$(Hz)** | **H-comp** | **V-Comp** | **H+V** |
| **(1)** | **(2)** | **(3)** | **(4)** | **(5)** | **(6)** |
| 5 | 3.53 | 0.341 | 0.220 | 0.323 | 0.56 |
| 6 | 4.23 | 0.286 | 0.194 | 0.286 | 0.48 |
| 7.5 | 5.29 | 0.233 | 0.171 | 0.251 | 0.42 |
| 10 | 7.06 | 0.165 | 0.146 | 0.213 | 0.36 |
| 12.5 | 8.83 | 0.136 | 0.130 | 0.193 | 0.32 |
| 15 | 10.59 | 0.113 | 0.119 | 0.177 | 0.29 |
| 17.5 | 12.35 | 0.097 | 0.113 | 0.163 | 0.27 |
| 20 | 14.12 | 0.090 | 0.106 | 0.153 | 0.26 |

.

## 3.3 Effects of Poisson's Ratio

To validate the above conclusions and also find out the Rayleigh-wave characteristics considering effects of Poisson's ratio, there are four homogeneous half-space models for which the seismic response is recorded at the epicentral distance. Homogeneous half-space models are (MH1-MH4) are shown in table 3.3. There is calculation of the velocity of P-wave, SV-wave for different Poisson's ratio for cutoff frequency 2.0 Hz, Rayleigh wave velocity, density and Poisson's ratio for four type of considered homogeneous half-space models. Figure 3.13a shows the seismic record of homogeneous half-space models with different Poisson's ratio using a point source earthquake at a depth of 7.5 km at an epicenter of 372 km. There is minor increase of Rayleigh wave amplitude with the reduction of Poisson's ratio.

Figure 3.13b, shows the spectral amplitudes are rise with decrease of Poisson's ratio. Figure 3.13c shows the ratio of focal depth and wavelength is constant for all Poisson's ratio using the focal depth of 7.5 km point source. Corresponding to maximum normalized spectral amplitude occurs at the constant value of $FD/\lambda = 0.63$ and the remaining other ratio before and after the $FD/\lambda = 0.63$ there is exponential reduction of normalized amplitude of the Rayleigh wave. So considering this point, we determine that the maximum energy of incident *SV*-wave adapts into energy of the Rayleigh wave at the critical distance when the when focal depth of point source earthquake is equal to 0.63 times to wavelength of the Rayleigh-wave.

**Table 3.3** Rheological parameter for different Poisson's ratio at cut-off frequency 2 Hz homogeneous half-space models

| **Homogeneous Model** | **$V_P$ (m/s)** | **$V_S$ (m/s)** | **$V_R$ (m/s)** | **$Q_P$** | **$Q_S$** | **Density ($kg/m^3$)** | **Poisson's ratio** |
|---|---|---|---|---|---|---|---|
| MH-1 | 5200 | 2874.40 | 2657.67 | 520.0 | 287.44 | 2800 | 0.28 |
| MH-2 | 5200 | 3000.00 | 2767.00 | 520.0 | 300.00 | 2800 | 0.25 |
| MH-3 | 5200 | 3115.55 | 2858.51 | 520.0 | 311.55 | 2800 | 0.22 |
| MH-4 | 5200 | 3184.33 | 2913.66 | 520.0 | 318.43 | 2800 | 0.20 |

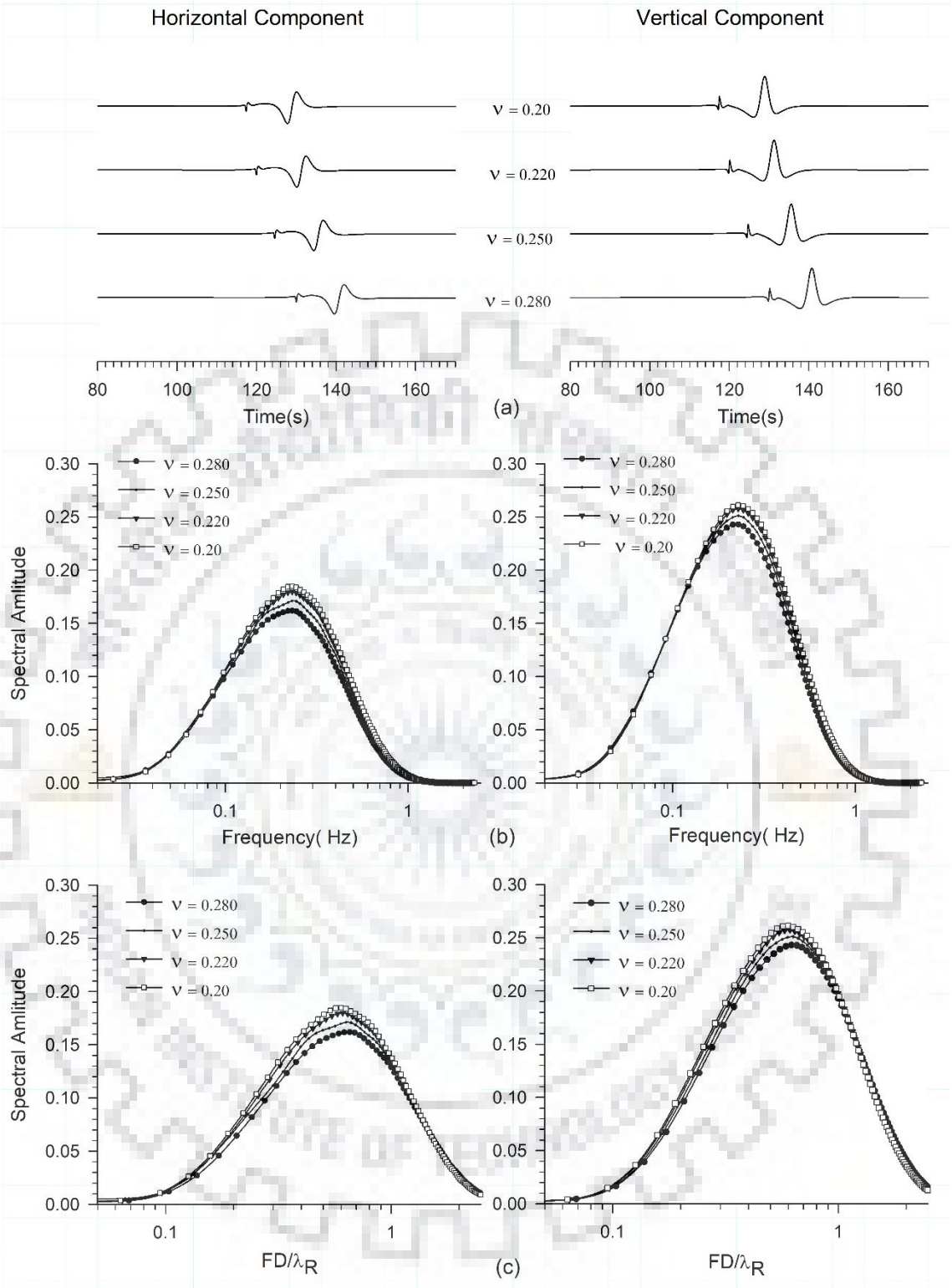


**Figure 3.13** (a) The responses at epicenter of 372 km for focal depth at 7.5 km and different Poisson's ratio (b) Plot of the spectra of Rayleigh wave for different Poisson's ratio (c) The spectral amplitude spectral amplitude of Rayleigh wave with the ratio of focal depth to the wavelength of Rayleigh wave

## 3.4 Effects of Duration of STF

Other case to validate the above conclusion is the effects of duration of STF on the propagation and conversion of energy of SV-wave in to energy of the Rayleigh-wave. The seismic records of the homogenous model (MH-2) were computed using different cut-off frequency in the Gabor wavelet. The decrease of cut-off frequency is responsible for the decrease of frequency bandwidth of STF and increase of duration of the Gabor wavelet. The used cut-off frequency in the Gabor wavelet are 1.5, 1.75, 2.0 and 2.5 Hz. Figure 3.14a&b shows the Gabor wavelet and corresponding spectra for cut-off frequency in the Gabor wavelet as 1.5, 1.75, 2.0 and 2.5 Hz. A decrease in the bandwidth but an increase of spectral amplitude with the decrease of cut-off frequency can be inferred.

Figure 3.15a shows the seismic record of the MH2 homogeneous model at an epicentral distance of 372 km using focal depth 7.5 km point source. The duration of the STF increases then the amplitude in both horizontal and vertical component is also increases. The cut-off frequency is used in the Gabor wavelet as 1.5, 1.75, 2.0 and 2.5 Hz. This difference may be due to increase of amplitude of *SV*-wave with the drop of cut-off frequency in the Gabor wavelet. This interpretation is very clear in figure 3.14b, where normalized spectra of Rayleigh wave are plotted for different cut-off frequencies in Gabor wavelet. Similarly, figure 3.15c the ratio of focal depth and wavelength is constant for all the cut-off frequency using the 7.5 km focal depth point source corresponding to maximum normalized spectral amplitude occurs at the constant value of $FD/\lambda = 0.63$ and the remaining other ratio before and after the $FD/\lambda = 0.63$ there is exponential reduction.

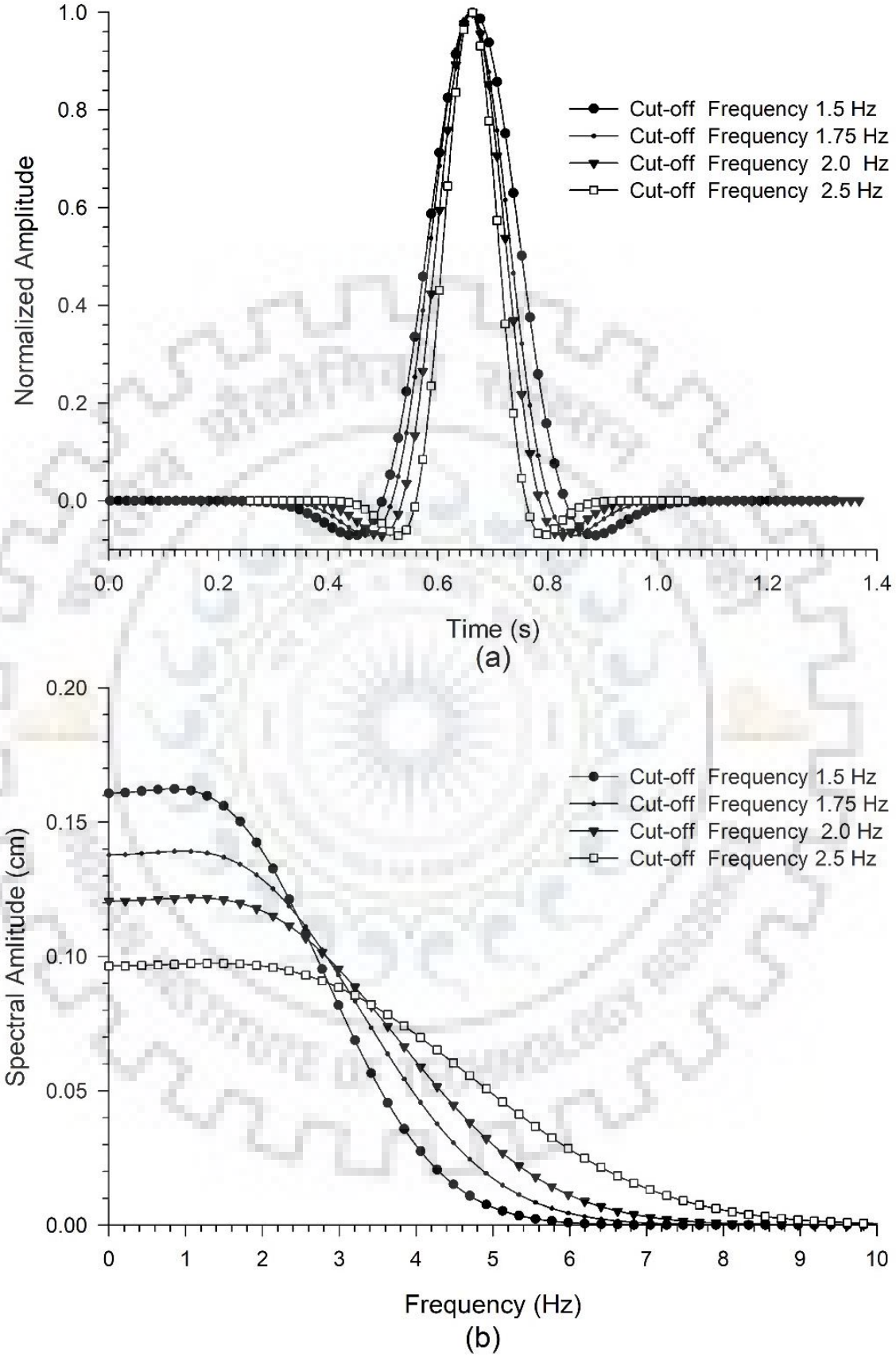


**Figure 3.14** Gabor wavelet for different cut-off frequency (b) The spectra of the source function with different cut-off frequency

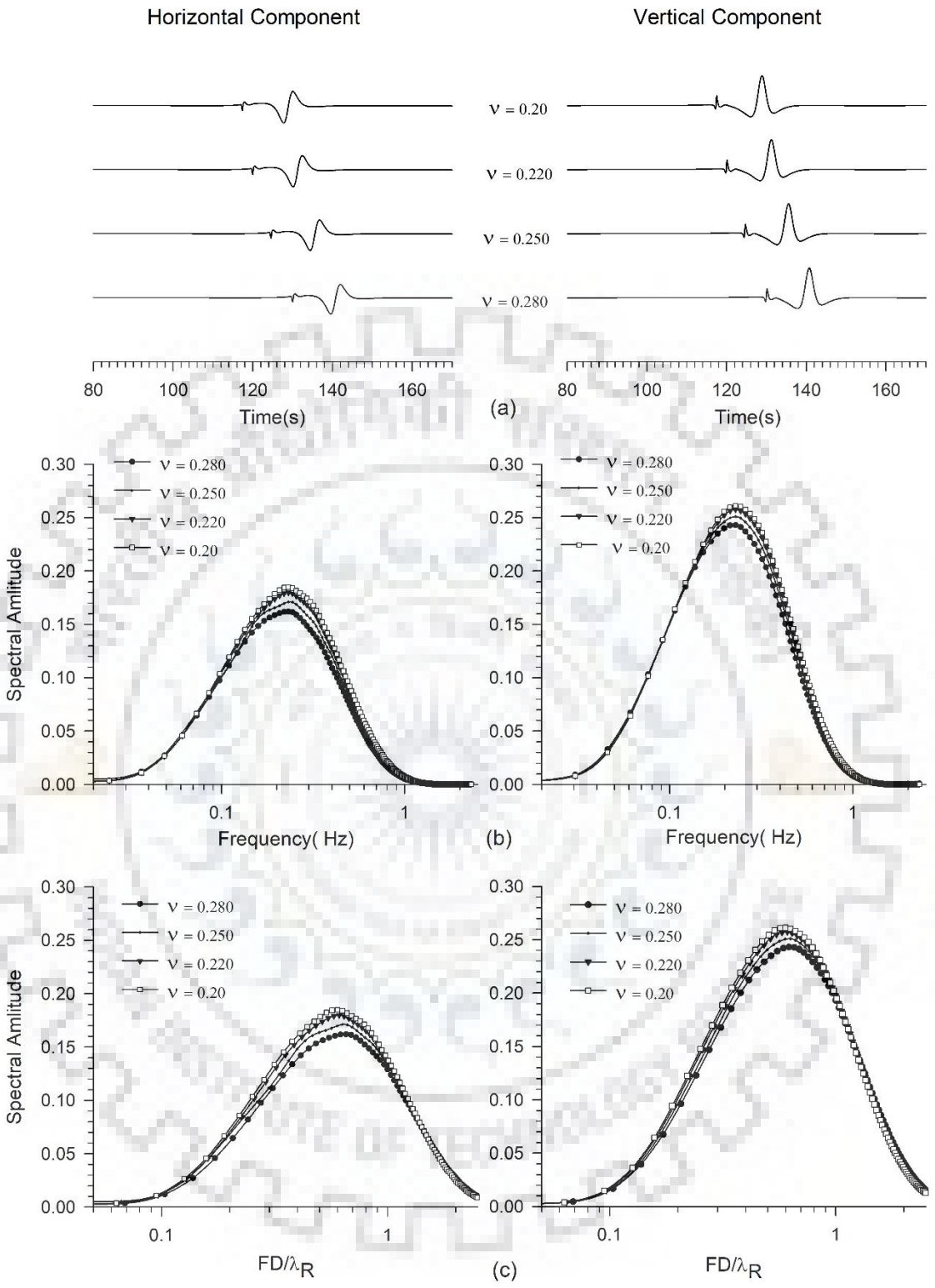


**Figure 3.15** The seismic record at epicenter of 372 km for different cut-off frequency using point source earthquake at focal depth 7.5 km (b) study of the spectra of only Rayleigh wave for different cut-off frequency at epicentral distance of 372 km (c) study of the spectral amplitude of Rayleigh wave part with the ratio of focal depth to the wavelength of Rayleigh wave

## 3.5 Rayleigh Wave Generation in Heterogeneous Half-Space

In order to infer the role of layered medium on the features of generated Rayleigh waves and their identification and separation from the SV-wave, the seismic responses of a model with crust and mantle are computed and analyzed. Table 3.3 gives the parameters for the considered heterogeneous half-space model with two layers. The grid size in X-direction was taken as 25 meter and in along the depth it was 25 meter up to depth of 21 km subsequently 60 meter. The time step of the order of 0.00216 second was taken to avoid the stability problem. The horizontal and vertical components of seismic responses were computed at 13 equidistance (31 km apart) receiver points. The first receiver was kept at the epicenter and the last one was kept at an epicentral distance 372 km.

**Table 3.4** Gives the rheological parameters of the heterogeneous half-space model

| **Earth layer** | **Thick-ness (km)** | **Vp (m/s)** | **$V_S$ (m/s)** | **$V_R$ (m/s)** | **Density ($kg/m^3$)** | **$Q_P$** | **$Q_S$** | **Poisson's ratio** |
|---|---|---|---|---|---|---|---|---|
| Crust | 33 | 5200 | 3000 | 2767 | 2800 | 520 | 300 | 0.25 |
| Mantle | --- | 7000 | 4000 | 3684 | 3200 | 700 | 400 | 0.25 |

Figure 3.16 seismic record of the heterogeneous half-space with 2 layer (crust and upper mantle) model using *SV*-wave dominated point source earthquake at a depth of 12.5 km. The dominant frequency used in the Gabor wavelet is 2.0 Hz. The seismic record at epicenter have signal only in the horizontal component and not in the vertical component, which is as per physics of the P- and SV-waves propagation in along the depth. The seismic records at an epicenter of 62 km reveals the incident P-wave, evanescence P-wave, SV-wave, generated Rayleigh wave along with the multiples of the body waves between free surface and moho discontinuity. Analysis of this figure reveals the dispersion of Rayleigh wave due to the presence of moho, particularly of those frequency whose wavelength is more than 33 km. The occurrence of dispersions and development of multiples between the free surface and the moho as well as development of other seismic phases, it is very difficult to separate out the Rayleigh.

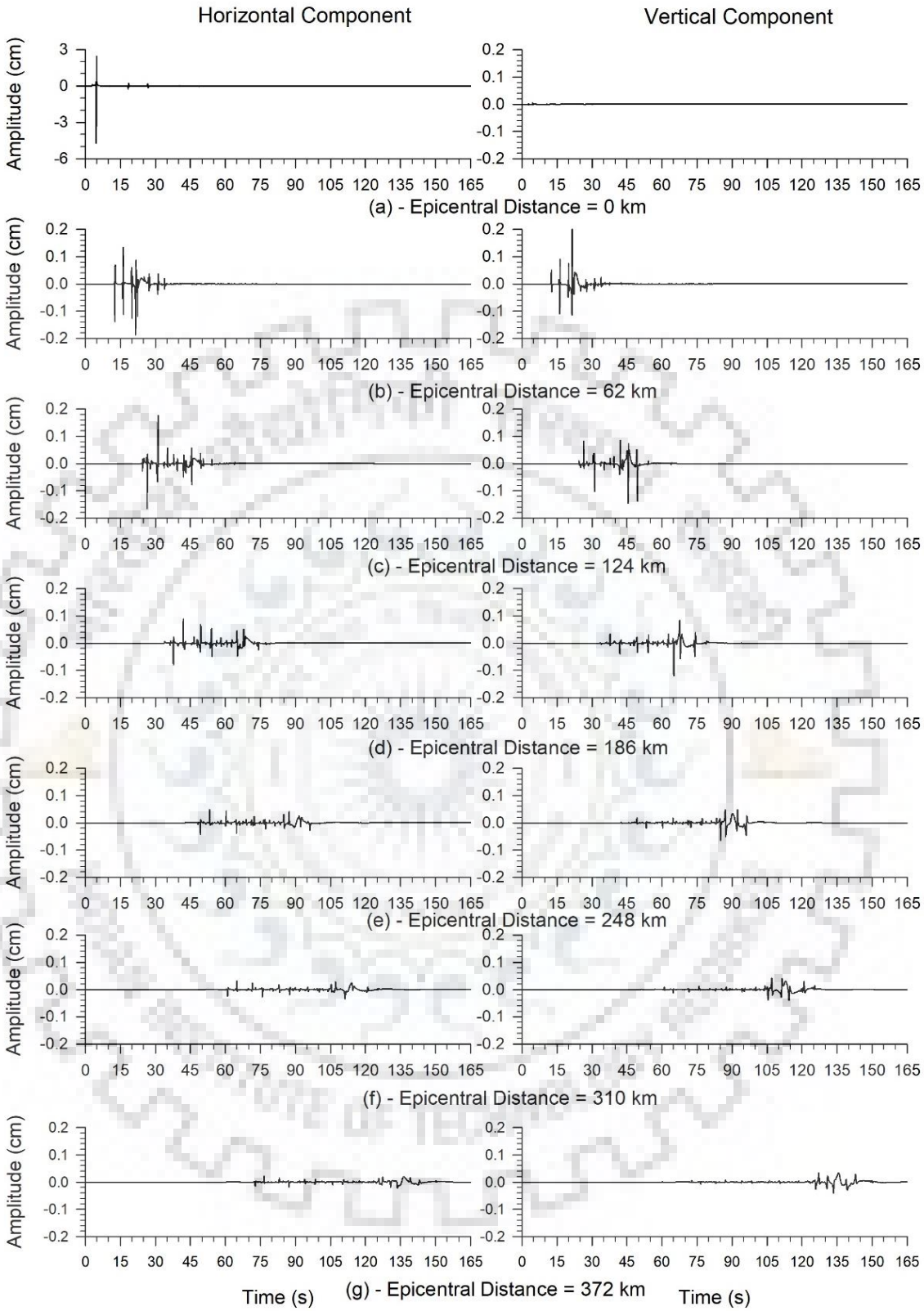


**Figure 3.16** The seismic record of heterogeneous half-space model at different epicenter using a SV-wave dominated point source earthquake at a depth of 12.5 km (Gabor wave is used as STF)

## 3.6 Summary

The simulated reciprocations of a P-SV wave related to a uniform half-space model by using various focal depth of point source and dominated with the SV-wave revealed Rayleigh wave generation at the critical distance. The reduction in spectral amplitude of generated Rayleigh waves when increase in focal depth may be due to the decrease of curvature of the wave front. The amplitude of Rayleigh wave initiated by the incoming P wave on the free surface is insignificant in contrast to that affected by the incoming SV wave. The observed comparative increase of amplitude of direct P wave and SV wave in contrast to the generated Rayleigh wave with increase of focal depth may be due to the reduction in amplitude of Rayleigh wave with higher values of depth of point source. The rate of reduction in evanescence P-wave with epicentral distance is lesser than the body waves.

A decrease of bandwidth for the generated Rayleigh wave can be observed when compared to higher values of focal depth. Further, there is almost linear reduction in spectral amplitude of Rayleigh waves with higher values of focal depth corresponding to the unit spectral amplitude of the incident SV wave at the epicenter. The largest spectral amplitude as unity amplitude of incident SV wave at the epicenter was produced for that wavelength for ratio which focal depth of point source earthquake to Rayleigh wave wavelength was about 0.63 for *SV*-wave source with Gabor wavelet as source time function. Further, there is almost exponential reduction in spectral amplitude corresponding to Rayleigh wave departing from the peak value of focal depth to wavelength ratio of Rayleigh wave. The analyzed results using different cut-off frequencies in the STF revealed increase of spectral amplitude of the Rayleigh wave with increase duration of the STF. A minor increase of spectral amplitude corresponding to Rayleigh wave is resulted in decrease of Poisson's ratio of the uniform half-space model.

# Chapter 4 : RAYLEIGH WAVE GENERATION IN HOMOGENEOUS MEDIUM USING RICKER WAVELET AS SOURCE TIME FUNCTION

## 4.1 Response of Homogeneous Model using Ricker Wavelet as STF

The simulated seismic record of the homogeneous half-space model using Gabor wavelet as STF in the previous chapter revealed the generation of Rayleigh wave as well as considerable variation of characteristics of the generated Rayleigh wave with change of focal depth, Poisson's ratio and duration of the Gabor wavelet. In order to study the effects of wavelet shape on the generated Rayleigh wave in homogeneous half-space, seismic responses of the same model using Ricker wavelet as STF are simulated and analyzed and presented in this chapter. The SV-wave is generated at the focus using shear stress $\sigma_{xz}$ in the form of the Ricker wavelet (Source time function) with dominant frequency 2.0 Hz (with the considerable frequency bandwidth 0.02 Hz – 6 Hz). The homogeneous half-space model is discretized with the variable grid size. The grid size in X-direction is taken as 25 meter and in vertical direction it was 25 meter up to depth of 21 km thereafter 60 meter. The time step of the order of 0.0025 second was taken to avoid the stability problem. The horizontal and vertical components of seismic responses were computed at 13 equidistance (31 km apart) receiver points. The first receiver was kept at the epicenter and the last one was kept at an epicentral distance 372 km.

### 4.1.1 Time-Domain Responses

In the following sub-sections, analysis of the characteristics of the Rayleigh wave generation by using point source earthquake at different focal depth using Ricker wavelet as STF is described.

#### 4.1.1.1 Focal Depth = 5.0 Km

Figure 4.1 shows the horizontal and vertical components of seismic record of the homogeneous half-space model using Ricker wavelet as STF to incorporate point source earthquake at a focal depth of 5.0 km. The Ricker wavelet STF used for the dominant frequency of 2 Hz. The seismic record at an epicenter of 31 km clearly reveals the incident P-wave, evanescence P-wave, SV-wave and the generated Rayleigh wave at the free

surface in a sequential order in both the horizontal and vertical components. A separation of Rayleigh wave from the direct incident SV-wave with an increase of epicentral distance can be inferred very easily. A complete separation of Rayleigh wave with the SV-wave can be seen at epicentral distance 372 km.

#### 4.1.1.2 . Focal Depth = 6.0 Km

The horizontal (x) component and vertical (y) component of seismic record of the homogeneous half-space model by *SV*-wave dominated point source at focal depth 6.0 km is shown in figure 4.2. Again, the response at epicenter (at 0 km) has signal only in the horizontal component and not in the vertical component (result not shown here). The seismic record at an epicenter of 31 km clearly shows the direct P-wave, evanescence P-wave, SV-wave and the generated Rayleigh wave at the free surface in a chronological order in both the horizontal component and vertical component. The Rayleigh wave is mixed with the SV-wave. However, both the SV-wave and Rayleigh wave can be seen since there is a single wavelet corresponding to both the waves.

Similarly, figures 4.3 and 4.8 show the horizontal (x) and vertical (z) components of seismic record of homogeneous half-space model for following focal depths 7.5 km to 20.0 km (6 cases), respectively. In all the cases, Rayleigh waves can be identified, even at an epicenter of 31 km, except focal depth is more than 12.5 km. When focal depth is more than 12.5 km, the amplitude of generated Rayleigh wave is too less as compared to the direct incident SV-wave. Now, the analysis of figures 4.3- Figure 4.8 reflects that there is reduction of amplitude of the generated Rayleigh waves with an increase of focal depth, in the case of Ricker wavelet also. However, Rayleigh wave can be identified after an epicenter of 124 km in the cases where focal depth is more than 12.5 km. But, the Rayleigh wave is not totally separated from the SV-wave. There is a larger the duration of wavelet of Rayleigh wave with an increase of focal depth. This may be due to the reduction of frequency content in the generated Rayleigh wave. However, in all the cases, the Rayleigh waves are well parted from the SV-wave only at epicenter of 372 km.

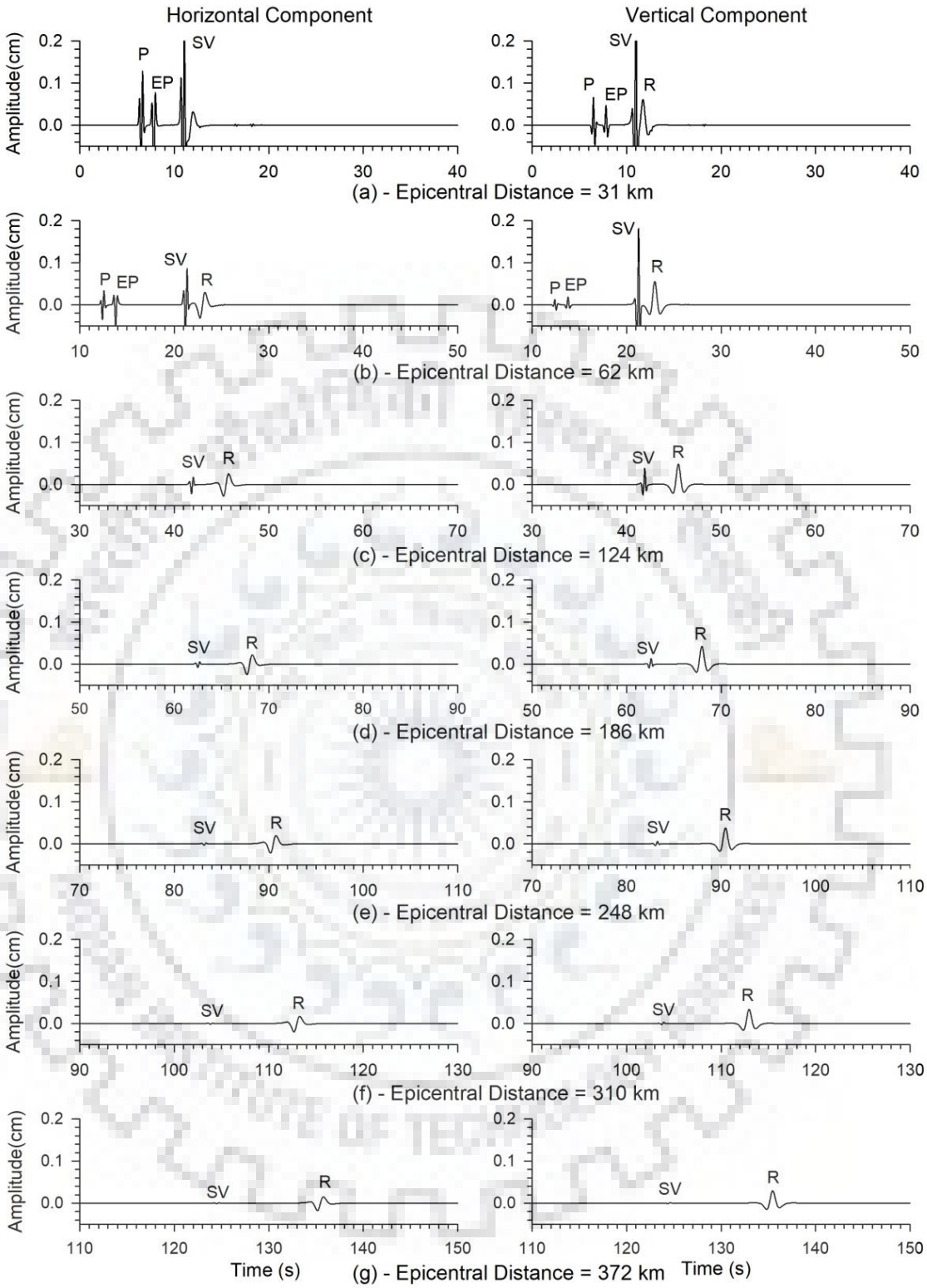


**Figure 4.1** The seismic record of homogeneous half-space model at different epicenter using a SV-wave dominated point source earthquake at a focal depth of 5.0 km (Ricker wave is used as STF)

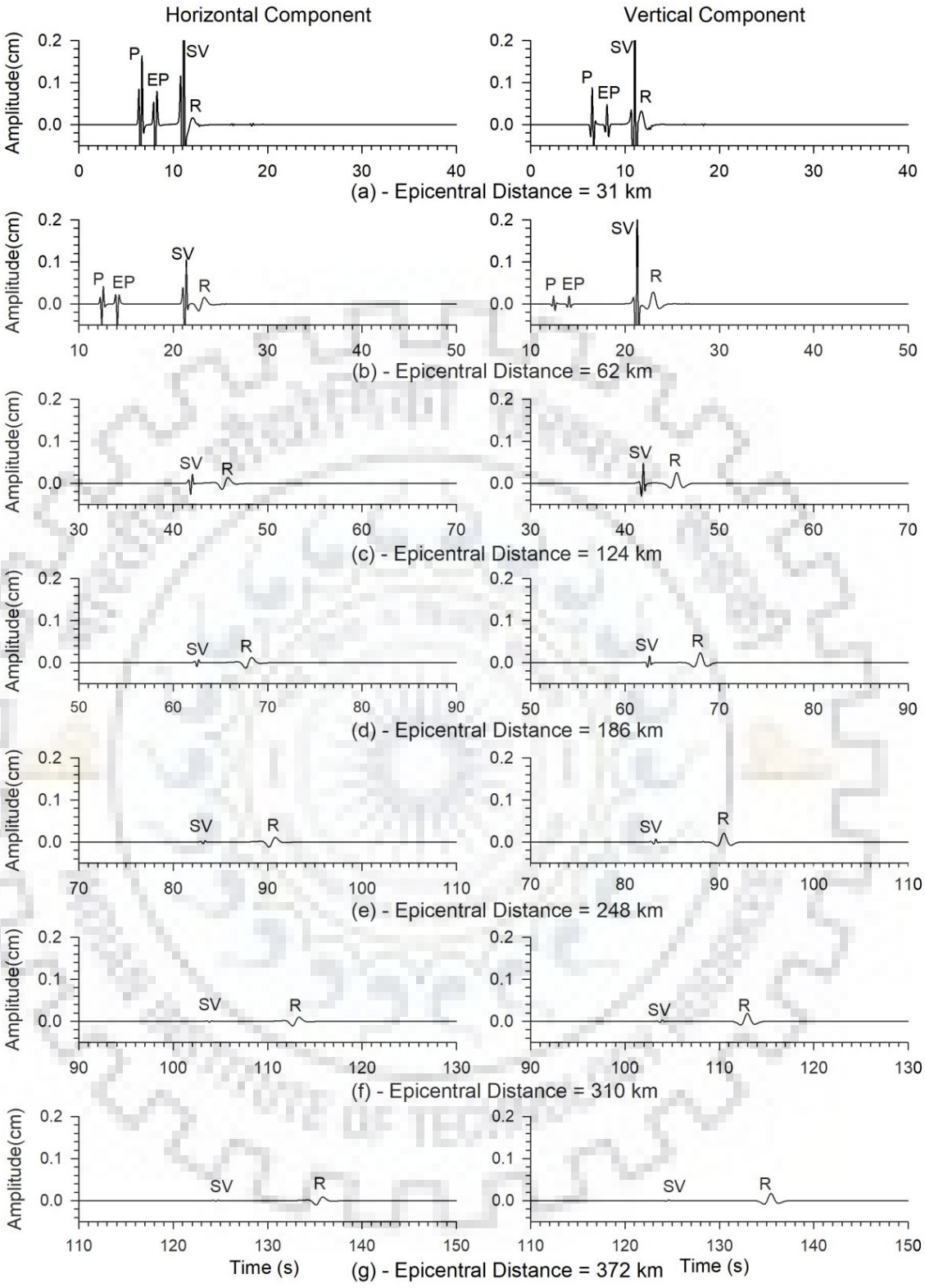


**Figure 4.2** The seismic record of homogeneous half-space model at different epicenter using a SV-wave dominated point source earthquake at a focal depth of 6.0 km (Ricker wave is used as STF)

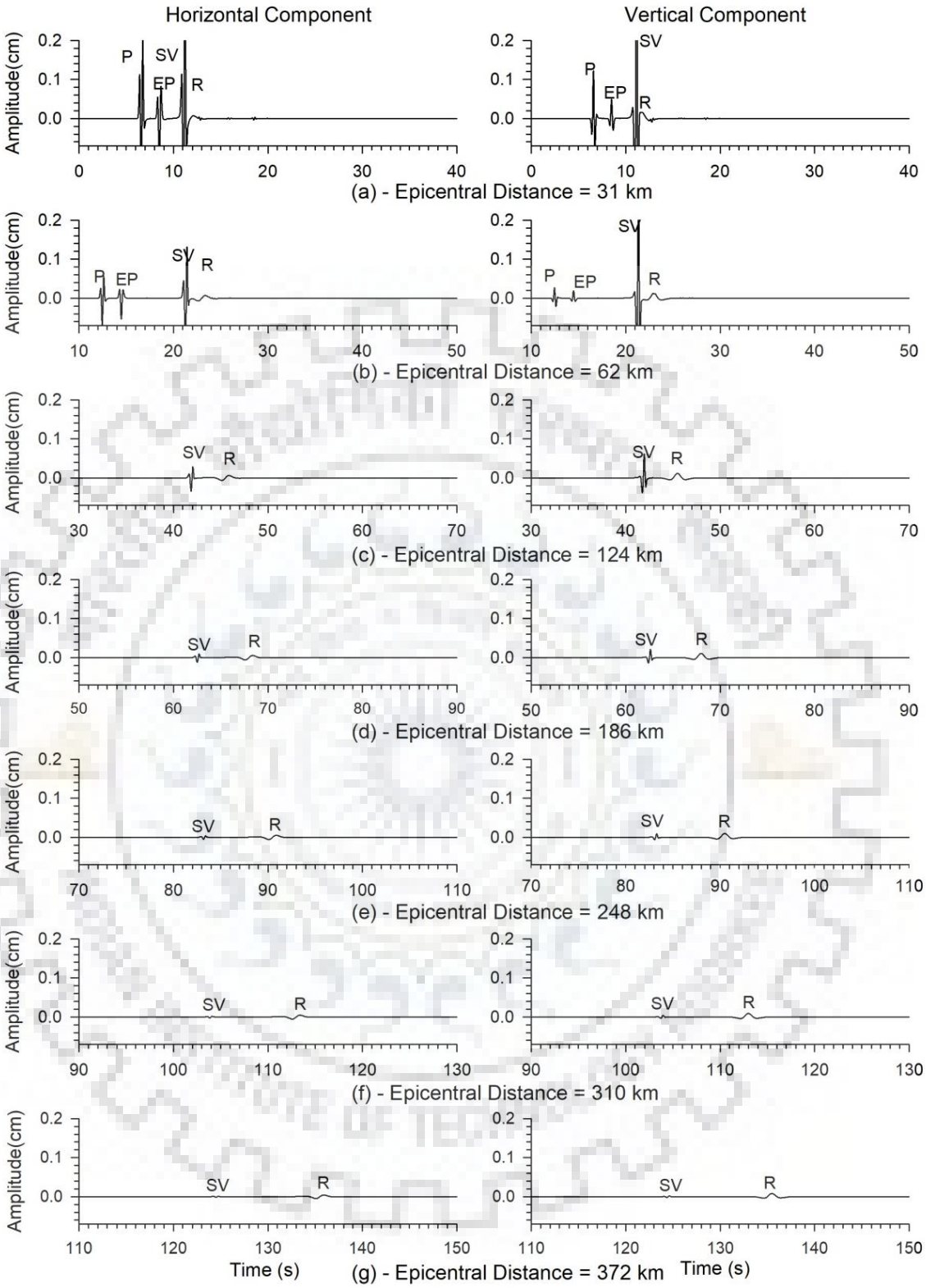


**Figure 4.3** The seismic record of homogeneous half-space model at different epicenter using a SV-wave dominated point source earthquake at a focal depth of 7.5 km (Ricker wave is used as STF)

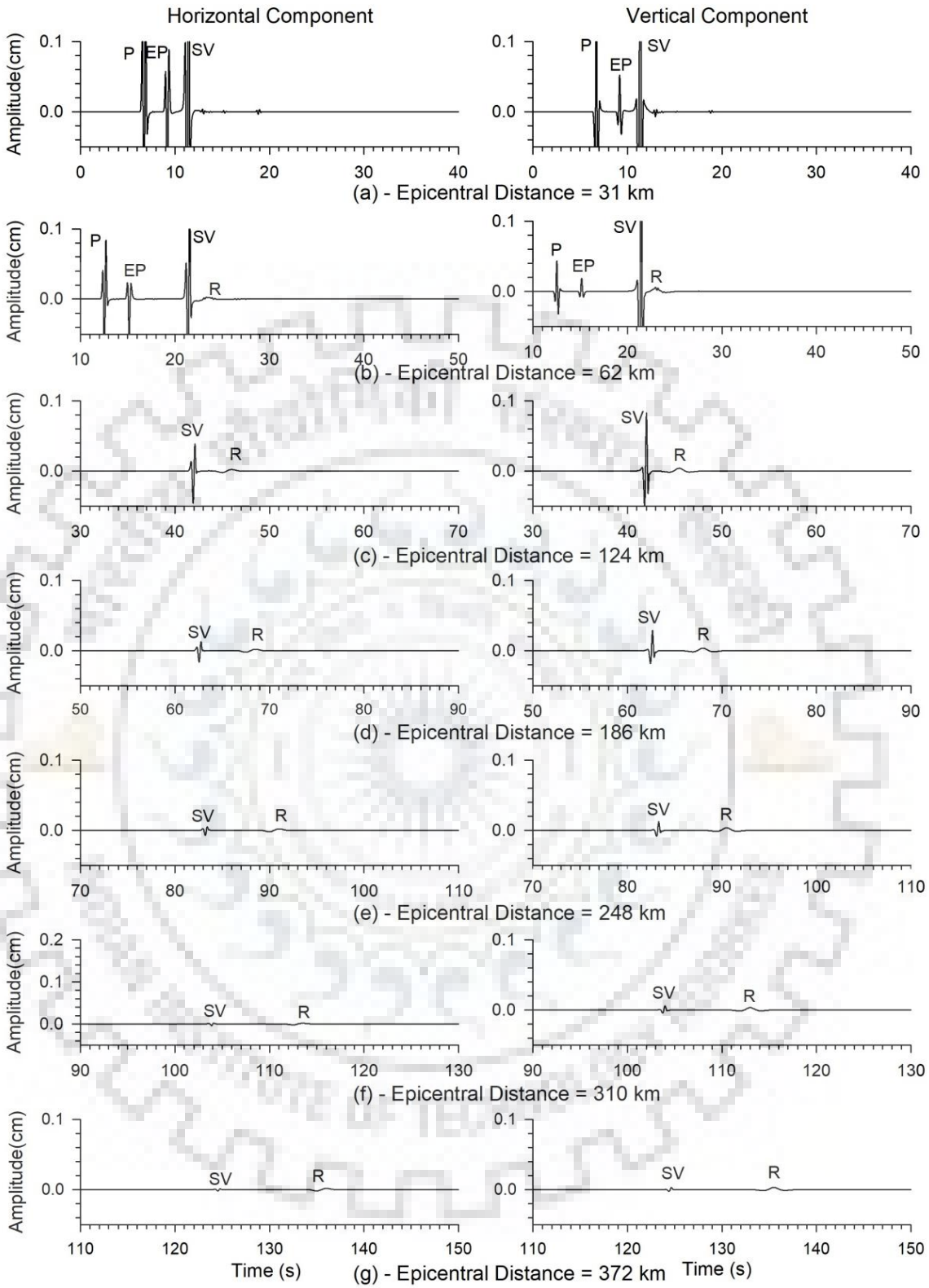


**Figure 4.4** The seismic record of homogeneous half-space model at different epicenter using a SV-wave dominated point source earthquake at a focal depth of 10.0 km (Ricker wave is used as STF)

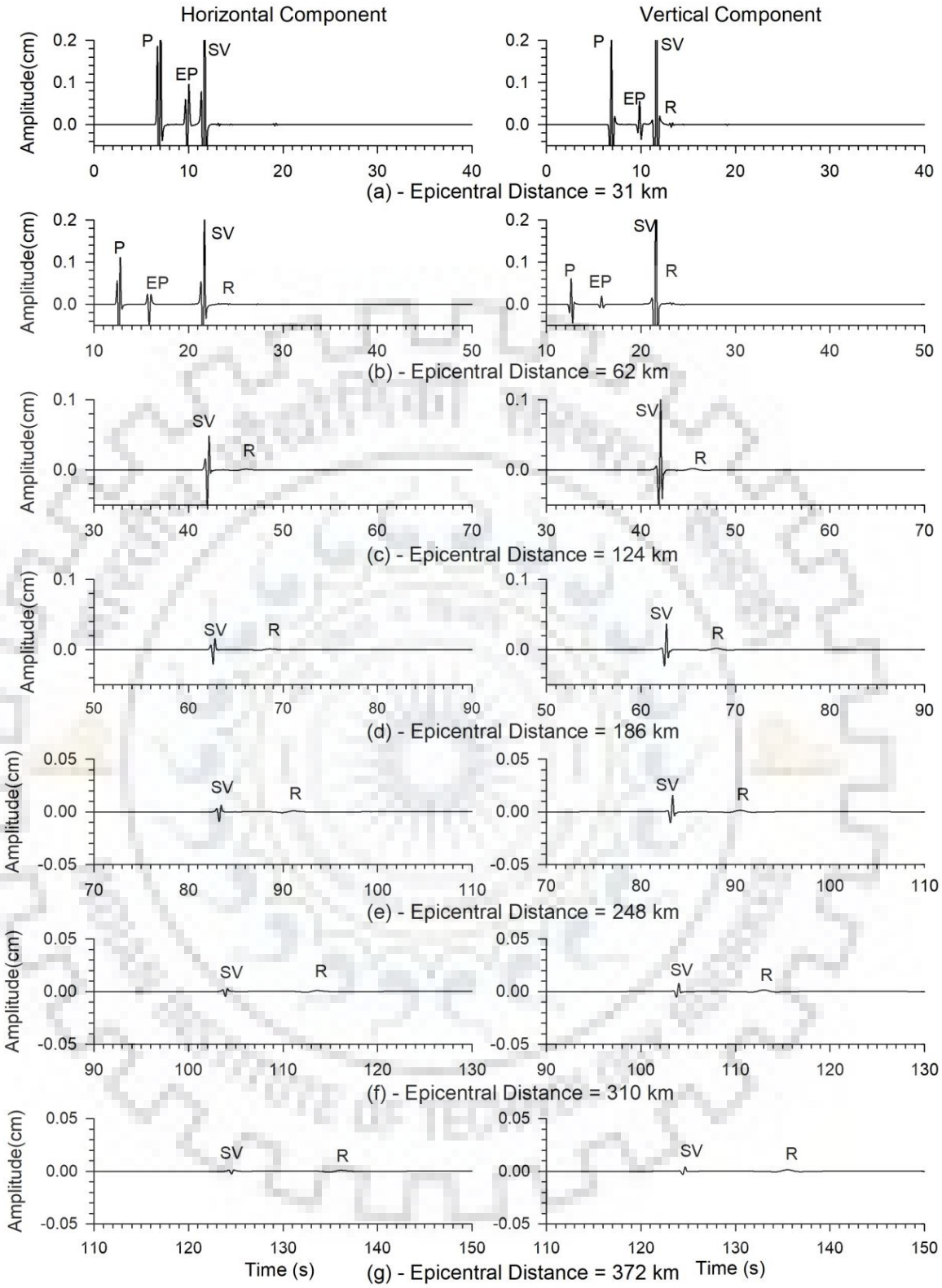


**Figure 4.5** The seismic record of homogeneous half-space model at different epicenter distances using a SV-wave dominated point source earthquake at a focal depth of 12.5 km (Ricker wave is used as STF)

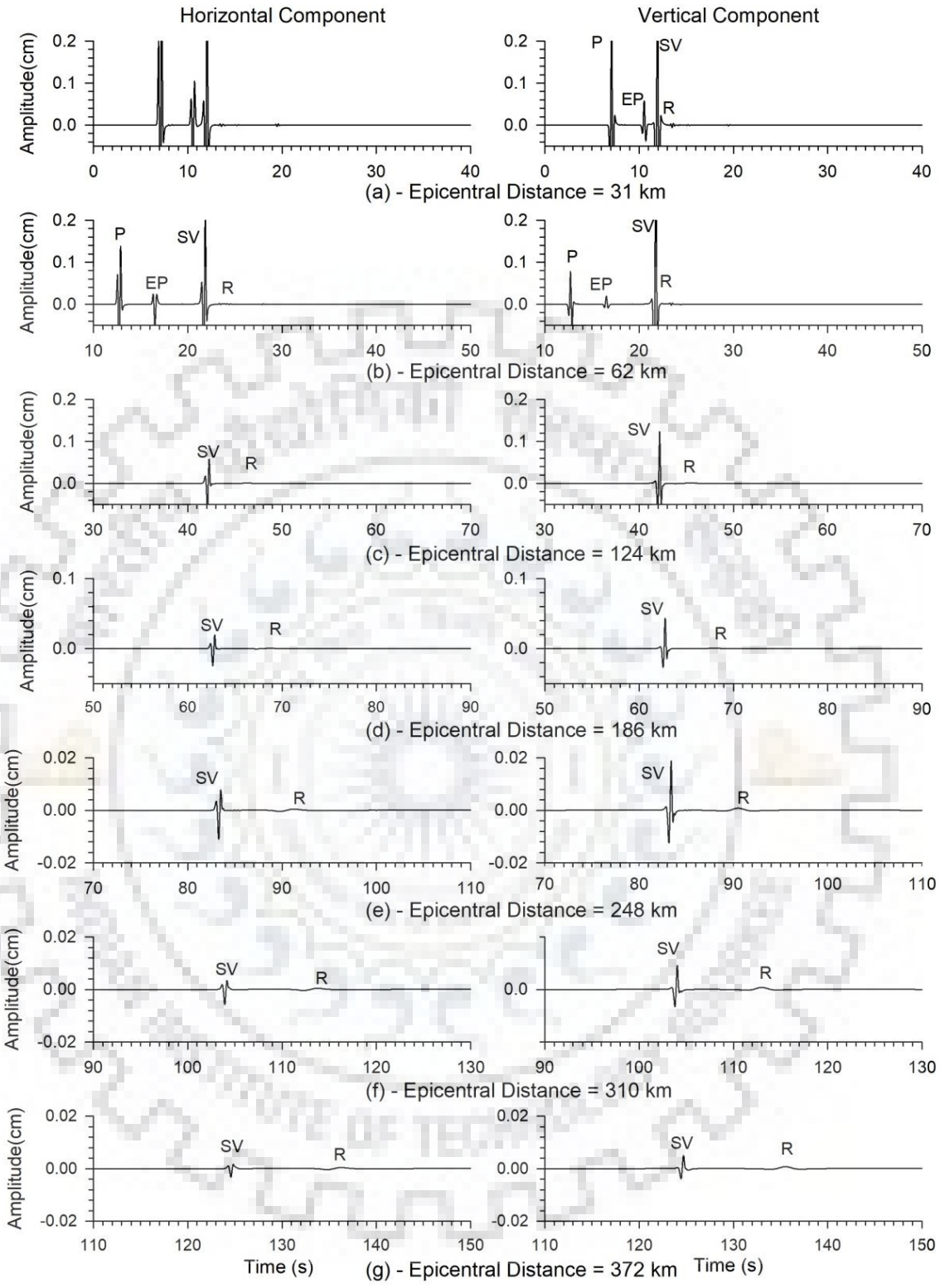


**Figure 4.6** The seismic record of homogeneous half-space model at different epicenter using a SV-wave dominated point source earthquake at a focal depth of 12.5 km (Ricker wave is used as STF)

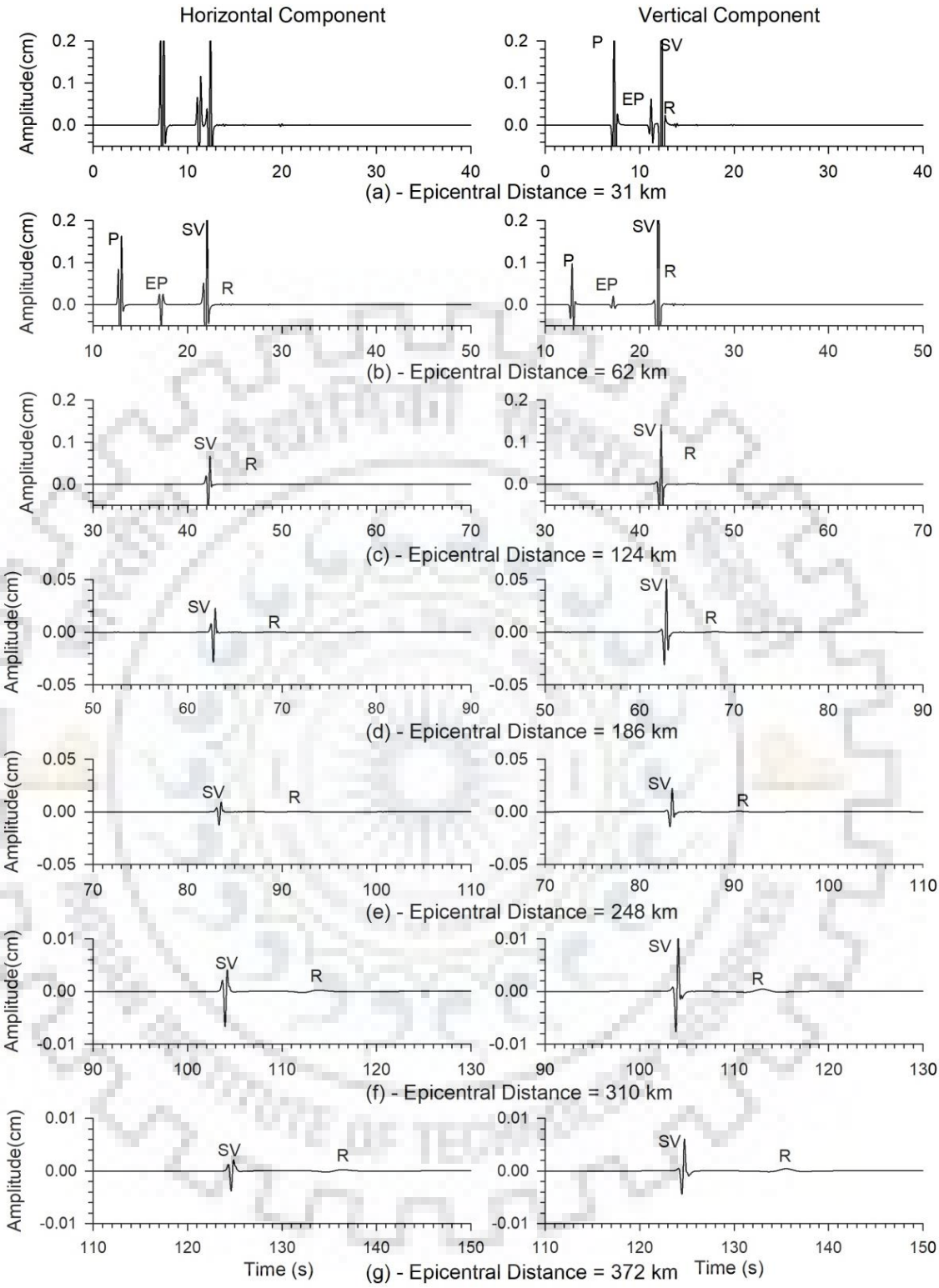


**Figure 4.7** The seismic record of homogeneous half-space model at different epicenter using a SV-wave dominated point source earthquake at a focal depth of 17.5 km (Ricker wave is used as STF)

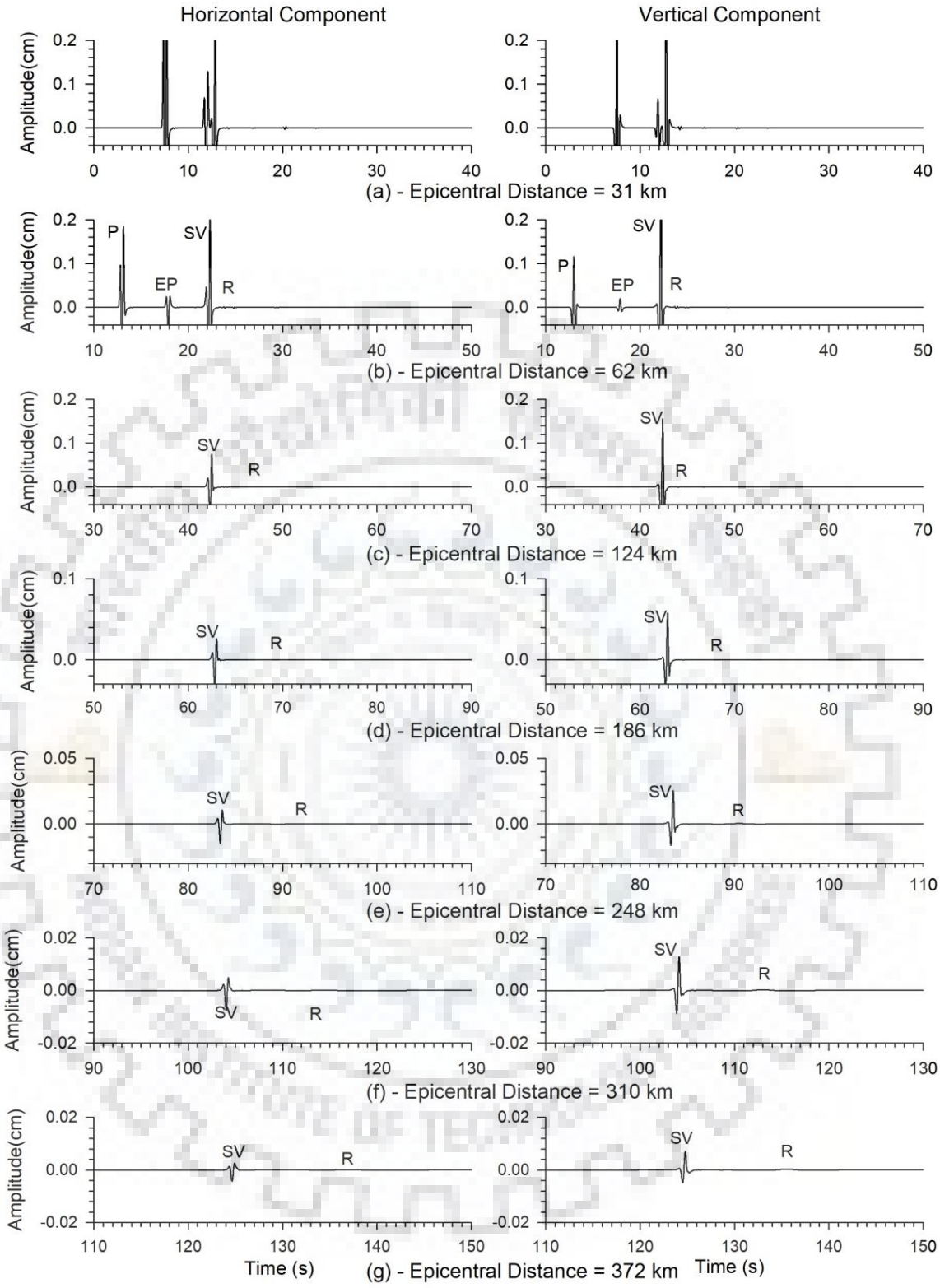


**Figure 4.8** The seismic record of homogeneous half-space model at different epicenter using a SV-wave dominated point source earthquake at a depth of 20.0 km (Ricker wave is used as STF)

### 4.1.2 Analysis of Simulated Results

Figure 4.9a show the computed seismic record at an epicenter of 372 km corresponding to the different focal depths of point earthquake source. The analysis of figure 3.9a shows the drop of amplitude of Rayleigh wave with increase of focal depth. Further, increase of the focal depth there is reduction of frequency content in the Rayleigh wave, which is reflected in the form of widening of the wavelet. In order to achieve the spectral amplitude of generated Rayleigh wave corresponding to the unit spectral amplitude of the incident SV-wave at the epicenter, the spectra of traces recorded at the epicentral distance of 372 km are normalized with the spectra of the traces recorded at the epicenter. In figure 4.9b there is consideration of only Rayleigh wave part from the record of different focal depth at an epicentral distance of 372 km and plot the graph between the normalized spectral amplitude (normalized with the spectra of STF) and the frequency.

An analysis of figure 4.9b shows that the reduction of frequency bandwidth of the generated Rayleigh wave with an increase of focal depth of point source. Further, the frequency corresponding to the peak normalized spectral amplitude is also reduced with increasing focal depth. Figure 4.10a clearly shows that as the focal depth increases then the almost exponential drop of peak frequency in horizontal and vertical component. On an average, rise of spectral amplitude in lower frequency and drop in higher frequency with respect to the dominant frequency can be observed. To see whether there is maximum translation of energy of the SV-wave in the energy of the Rayleigh wave corresponding to particular frequency, normalized spectral amplitude at an epicenter of 372 km and the $FD/\lambda$ ratio for different focal depths and shown in figure 4.9c (where FD is focal depth and $\lambda$ is the wavelength of the Rayleigh wave). The ratio of focal depth and wavelength is constant for all the focal depth corresponding to maximum normalized spectral amplitude occurs at the constant value of $FD/\lambda = 0.63$ and the remaining other ratio before and after the $FD/\lambda = 0.63$ there is exponential reduction of normalized amplitude of the Rayleigh wave. So, considering this point, we conclude that at and the large amount energy of *SV*-wave adapts into the Rayleigh wave energy when focal depth of point source is equal to 0.63 times to that of the wavelength of Rayleigh-wave.

Further, figure 4.10b depicts that for different focal depth and the normalized spectral amplitude where the peak of frequency is occur. There is the horizontal and vertical component clearly so that the normalized amplitude of vertical component is 1.5

more than the horizontal component. The reduction of the normalized amplitude with increasing the focal depth. The reduction in normalized amplitude in both the component (horizontal and vertical) is almost exponentially.

Similarly, in case of the Gabor wavelet, the conversion of energy of the incident SV-wave at the critical distance in to the Rayleigh wave at the prominent frequency. To calculate the conversion of the energy of incident SV-wave at the critical distance, we have to consider the divergence and damping effects. Calculation of parameter is similar in case of the Gabor wavelet STF .

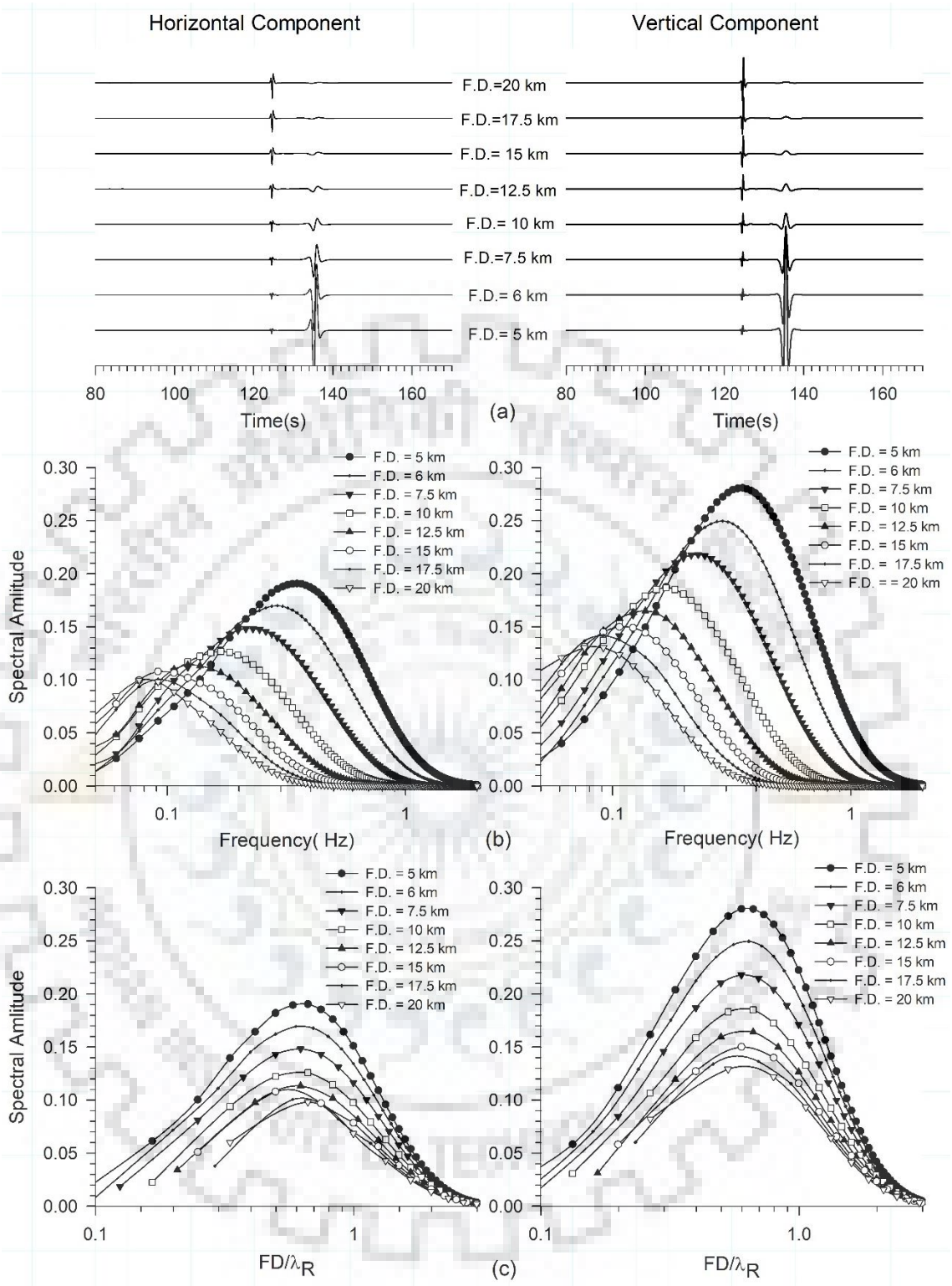


**Figure 4.9** (a) The seismic record for different focal depths at epicenter of 372 km (b) Analysis of the spectra of only Rayleigh wave at epicenter of 372 km for different focal depths (c) Analysis of the spectral amplitude of only Rayleigh wave at epicenter of 372 km with the ratio of different focal depth to the wavelength of Rayleigh wave

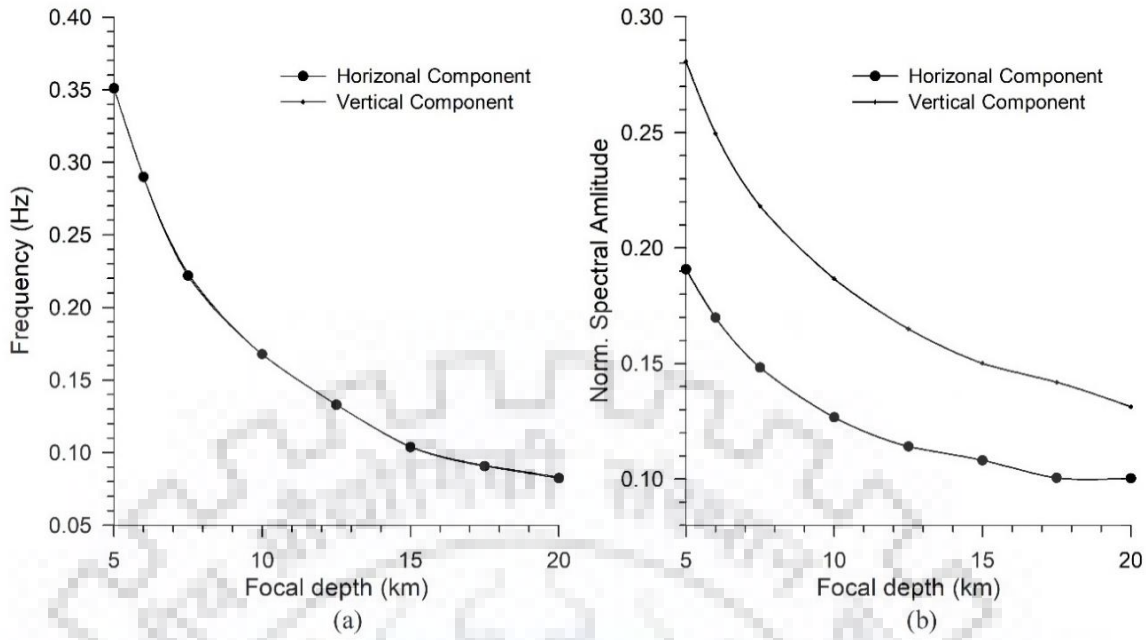


**Figure 4.10** (a) The peak frequency of horizontal and vertical component at epicentral distance of 372 km for different focal depths (b) The maximum normalized spectral amplitude corresponding to peak frequency for different focal depth (Ricker wave is used as STF)

Than consideration of the similar formula used in case of the Gabor wavelet. The energy conversion of the incident SV-wave at the critical distance in to the Rayleigh wave with the Gabor wavelet as a STF is calculated by adding the peak normalized amplitude of the both component. Table 4.1 clearly show that the reduction of the converted energy of the incident SV-wave to Rayleigh wave at the critical distance with increase in the focal depth. The largest spectral amplitude of the prominent frequency of Rayleigh wave for unit amplitude of the incident SV-wave at the critical distance was obtained as 47.1% and 23.1% corresponding to focal depths 5 km and 20 km, respectively.

Table 4.1 also show the comparisons of the peak normalized amplitude of the Gabor and Ricker wavelet which clearly shows that the energy relies in case of the Gabor wavelet is more than the Ricker wavelet and the average of the both wavelet converted energy at the critical distance from the incident SV-wave to Rayleigh wave.

**Table 4.1** The variation of obtained prevailing frequency ($F_P$), amplitude in the horizontal (H) and vertical (V) components of Rayleigh wave of frequency $F_P$ at the critical distance with focal depth (F.D.) corresponding to the unit spectral amplitude of the incident SV-wave at the critical distance (C.D.) in the Gabor wavelet and Ricker Wavelet cases.

| **F.D.** | **C.D.** | **$F_P$ (Hz), amp. in H- & V-comp. of R-wave at $F_P$ at critical dist. (Gabor wavelet case)** | | | | **$F_P$ (Hz), amp. in H- & V-comp. of R-wave at $F_P$ at critical dist. (Ricker wavelet case)** | | | | **Avg. of cols. 6 &10** |
|---|---|---|---|---|---|---|---|---|---|---|
| **(km)** | **(km)** | **$F_P$ (Hz)** | **H-comp** | **V-comp** | **H+V** | **$F_P$ (Hz)** | **H-comp** | **V-comp** | **H+V** | |
| **(1)** | **(2)** | **(3)** | **(4)** | **(5)** | **(6)** | **(7)** | **(8)** | **(9)** | **(10)** | **(11)** |
| 5 | 3.53 | 0.341 | 0.220 | 0.32 | 0.56 | 0.351 | 0.190 | 0.280 | 0.47 | 0.50 |
| 6 | 4.23 | 0.286 | 0.194 | 0.28 | 0.48 | 0.289 | 0.169 | 0.249 | 0.42 | 0.45 |
| 7.5 | 5.29 | 0.233 | 0.171 | 0.25 | 0.42 | 0.222 | 0.148 | 0.218 | 0.36 | 0.39 |
| 10 | 7.06 | 0.164 | 0.146 | 0.21 | 0.36 | 0.167 | 0.126 | 0.186 | 0.31 | 0.34 |
| 12.5 | 8.83 | 0.136 | 0.130 | 0.19 | 0.32 | 0.133 | 0.114 | 0.165 | 0.28 | 0.30 |
| 15 | 10.59 | 0.112 | 0.118 | 0.17 | 0.29 | 0.103 | 0.108 | 0.150 | 0.26 | 0.27 |
| 17.5 | 12.35 | 0.096 | 0.112 | 0.16 | 0.27 | 0.090 | 0.100 | 0.141 | 0.24 | 0.26 |
| 20 | 14.12 | 0.090 | 0.106 | 0.15 | 0.26 | 0.082 | 0.100 | 0.131 | 0.23 | 0.24 |

## 4.2 Effects of Poisson's Ratio

To further validate the above conclusions in the Ricker wavelet as the STF and also find out the Rayleigh-wave characteristics considering effects of Poisson's ratio, there are four homogeneous half-space models for which the seismic response is recorded at the epicentral distance. The different homogeneous half-space models are (MH1-MH4) are shown in table 3.2. There is calculation of the velocity of P-wave, SV-wave for different Poisson's ratio for cutoff frequency 2.0 Hz, Rayleigh wave velocity, density and Poisson's ratio for different type of considered homogeneous half-space models. Figure 3.13a show the seismic record of homogeneous half-space models with different Poisson's ratio using a point source earthquake at a depth of 7.5 km at an epicenter of 372 km. There is minor increase of amplitude of Rayleigh wave with the reduction of Poisson's ratio.

The normalized amplitude of Rayleigh wave in both the horizontal component and vertical component considering the effects of Poisson's ratio in time domain is very clear in figure 3.13b, where spectral amplitudes are rise with decrease of Poisson's ratio. Figure 3.13c shows the ratio of focal depth and wavelength is constant for all Poisson's ratio using the focal depth of 7.5 km point source. Corresponding to maximum normalized spectral amplitude occurs at the constant value of $FD/\lambda = 0.63$ and the remaining other ratio before and after the $FD/\lambda = 0.63$ there is exponential reduction of normalized amplitude of the Rayleigh wave. So considering this point, we conclude that the maximum energy of *SV*-wave adapts into the Rayleigh wave when focal depth equal to 0.63 times to that of the Rayleigh-wave wavelength.

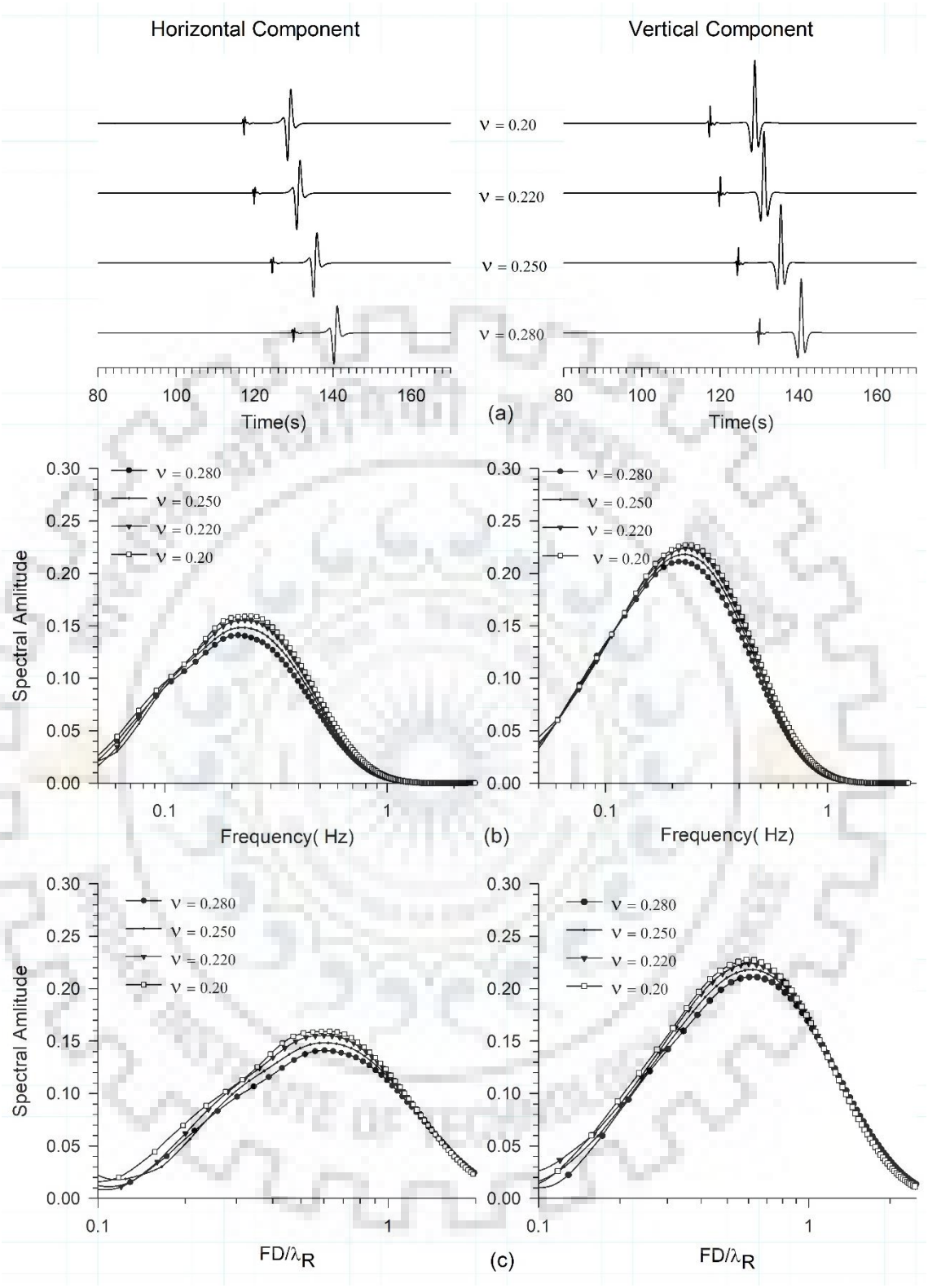


**Figure 4.11** (a) The seismic record at epicenter of 372 km corresponding focal depth and different Poisson's ratio (b) Plot of the spectra of Rayleigh wave for different Poisson's ratio (c) Plot of the spectral amplitude of Rayleigh wave with the ratio of focal depth to the wavelength of Rayleigh wave

## 4.3 Effects of Duration of STF

Other case to validate the above conclusion is the effects of duration of STF on the propagation of SV-wave energy in to Rayleigh-wave energy. The seismic responses of the homogenous model (MH-2) were computed using different cut-off frequency in the Gabor wavelet. The decrease of cut-off frequency is responsible for the decrease of frequency bandwidth of STF and increase of duration of the Gabor wavelet. The used cut-off frequency in the Gabor wavelet are 1.5, 1.75, 2.0 and 2.5 Hz. Figure 4.12a&b shows the Gabor wavelet and corresponding spectra for cut-off frequency in the Gabor wavelet as 1.5, 1.75, 2.0 and 2.5. A decrease in the bandwidth but an increase of spectral amplitude with the decrease of cut-off frequency can be inferred.

Figure 4.13a shows the seismic record of the MH2 homogeneous model at an epicenter of 372 km using focal depth 7.5 km point source. The duration of the STF increases then the amplitude in both horizontal and vertical component is also increases. Used cut-off frequency in the Gabor wavelet as 1.5, 1.75, 2.0 and 2.5 Hz. This difference may be due to increase of amplitude of *SV*-wave with the decrease of cut-off frequency in the Gabor wavelet. This interpretation is very clear in figure 3.14b, where normalized spectra of Rayleigh wave are plotted for different cut-off frequencies in Gabor wavelet. Similarly, figure 4.13c the ratio of focal depth and wavelength is constant for all the cut-off frequency using the 7.5 km focal depth point source corresponding to maximum normalized spectral amplitude occurs at the constant value of $FD/\lambda = 0.63$ and the remaining other ratio before and after the $FD/\lambda = 0.63$ there is exponential reduction. For example, there is around 20% and 14% of the SV-wave energy conversion in to Rayleigh wave energy corresponding to the dominant frequency in the STF as 1.5 Hz and 2.5 Hz, respectively.

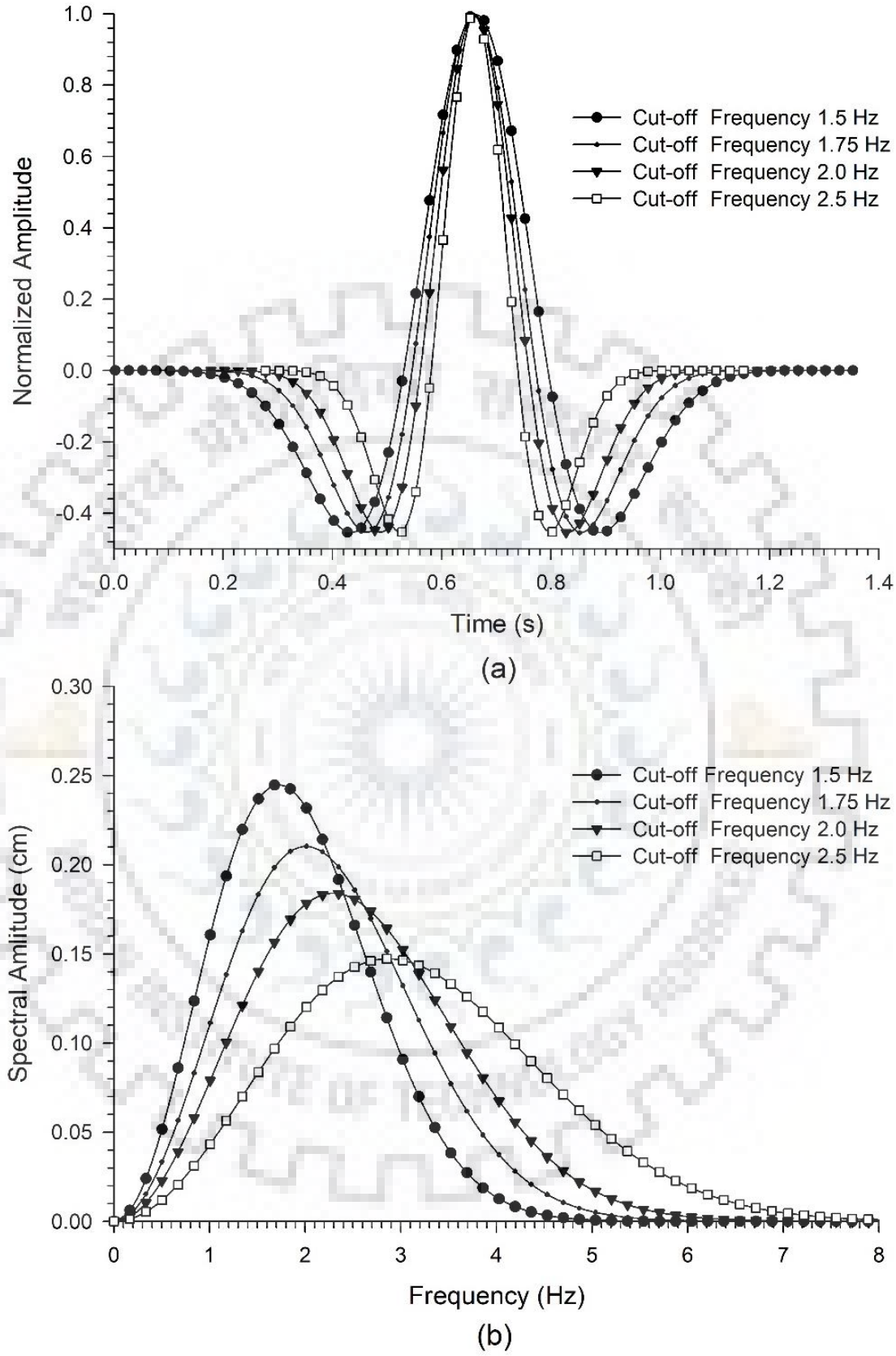


**Figure 4.12** (a) Ricker wavelet for different cut-off frequency (b) The spectra of the source function with different cut-off frequency

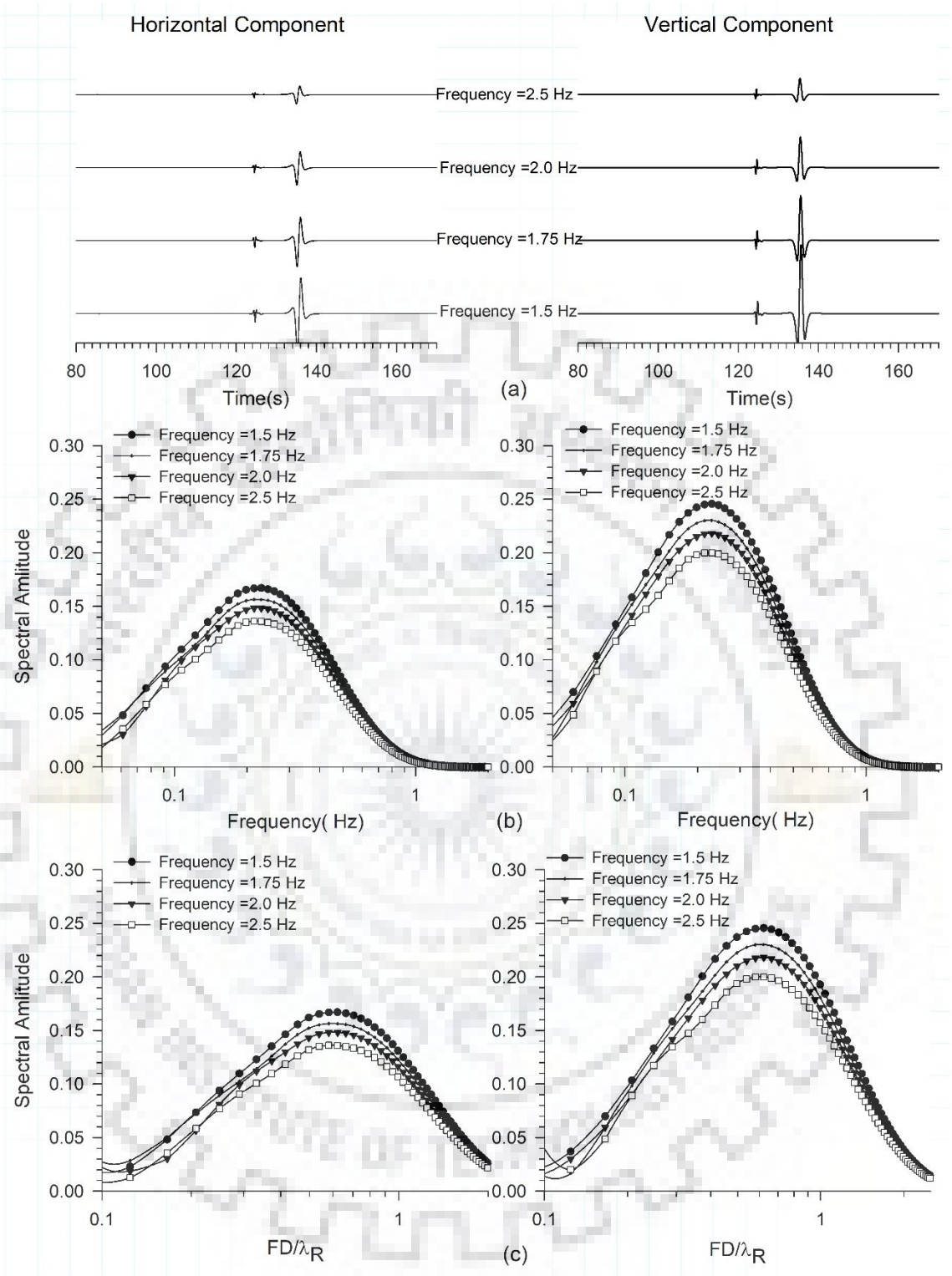


**Figure 4.13** The seismic record at epicenter of 372 km corresponding to different cut-off frequency using point source earthquake at focal depth 7.5 km (b) Study of the spectra of only Rayleigh wave for different cut-off frequency at epicenter of 372 km (c) Study of the spectral amplitude of only Rayleigh wave with the ratio of focal depth to the wavelength of Rayleigh wave

## 4.4 Summary

The simulated P-SV wave records of a homogeneous half-space model at epicenral distance of 372 km using different focal depth and Ricker wavelet as STF also revealed that the generation of Rayleigh wave at the critical distance. The highest spectral amplitude for unit amplitude of incident SV-wave at the epicenter for which the ratio of focal depth to wavelength of Rayleigh wave in Ricker wavelet is also similar to Gabor wavelet in the previous case which is around 0.63 in the case of *SV*-wave source as source time function. Further, there is almost exponential drop of spectral amplitude of Rayleigh wave passing from the highest value of ratio of focal depth to the Rayleigh wave wavelength. The obtained results using different cut-off frequencies in the STF shown an rise of spectral amplitude of the Rayleigh wave with increase of duration of the STF. In this case also, a minor rise of spectral amplitude of the Rayleigh wave is obtained with the reduction of Poisson's ratio in the homogeneous half-space model.

# Chapter 5 : DISCUSION AND CONCLUSIONS

The P-SV wave responses of a homogeneous half-space model using different Poisson's ratio, focal depth, source time function (STF) and duration of STF were simulated and analyzed. Although, the mode conversion of the incident SV-wave to P-wave at the free surface occurs between the epicenter and the critical distance, but the analysis of separated wave-form of the Rayleigh wave reveals that there is a single wavelet of Rayleigh wave and the shape is matching with the used STF. So, finally, it is concluded that coupling of the evanescence P-wave with the reflected SV-wave at the critical distance is responsible of the generation of Rayleigh wave. The observed reduction of time separation between the evanescence P-wave and the Rayleigh wave at a particular epicenter distance (say 31 km) Rayleigh wave generation at the critical distance is also supported by the increase of focal depth The largest spectral amplitude for unit amplitude of incident SV-wave at the epicenter was found in that wavelength (prominent frequency) for which the ratio of focal depth to Rayleigh wave wavelength was also about 0.63 in both the cases of used STFs.

The simulated results reveal a reduction of amplitude and frequency content and amplitude in the Rayleigh wave with the increase of focal depth, corresponding to the unit amplitude of the incident SV-wave at the epicenter. Now, question arise why there is reduction of amplitude and frequency content in the Rayleigh wave with a reduction of focal depth, if rheological parameters, free surface effects and frequency content in the STFs are same except the increase of critical distance from the epicenter. So, only possible reason behind the decrease of amplitude and frequency content in the Rayleigh wave with the increase of focal depth is the decrease of curvature of the wave-front with increase of focal depth.

Further, there is almost exponential reduction of spectral amplitude of Rayleigh waves with the increase of focal depth corresponding to the unit spectral amplitude of the incident SV-wave at the critical distance. The largest spectral amplitude of the prominent frequency of Rayleigh wave for unit amplitude of the incident SV-wave at the critical distance was obtained as 0.50, 0.45, 0.39, 0.33, 0.30, 0.27, 0.26 and 0.24 Corresponding to focal depth 5 km, 6 km, 7.5 km, 10 km, 12.5 km, 15 km, 17.5 km and 20 km respectively.

Further, there is almost exponential drop of spectral amplitude of Rayleigh wave departing from the inferred constant 0.63. A minor increase of spectral amplitude of the Rayleigh wave is attained with the decrease of Poisson's ratio in the homogeneous half-space and an increase of duration of STF.

# REFERENCES


1. Bard, P. Y., and Bouchon, M. (1980). "The seismic response of sediment-filled valleys. Part 1. The case of incident SH waves." *Bulletin of the seismological society of America*, 70(4), 1263-1286.
2. Boore, D. M. (1972). "Finite difference methods for seismic wave propagation in heterogeneous materials." *Methods in computational physics*, 11, 1-37.
3. Clayton, R., and Engquist, B. (1977). "Absorbing boundary conditions for acoustic and elastic wave equations." *Bulletin of the seismological society of America*, 67(6), 1529-1540.
4. Coutant, O., Virieux, J., and Zollo, A. (1995). "Numerical source implementation in a 2D finite difference scheme for wave propagation." *Bulletin of the Seismological Society of America*, 85(5), 1507-1512.
5. Ewing, W. M., Jardetzky, W. S., Press, F., and Beiser, A. P. T. (1957). "Elastic waves in layered media." *Physics Today*, 10, 27.
6. Gottschammer, E., and Olsen, K. (2001). "Accuracy of the explicit planar free-surface boundary condition implemented in a fourth-order staggered-grid velocity-stress finite-difference scheme." *Bulletin of the Seismological Society of America*, 91(3), 617-623.
7. Graves, R. W. (1996). "Simulating seismic wave propagation in 3D elastic media using staggered-grid finite differences." *Bulletin of the Seismological Society of America*, 86(4), 1091-1106.
8. Israeli, M., and Orszag, S. A. (1981). "Approximation of radiation boundary conditions." *Journal of computational physics*, 41(1), 115-135.
9. Levander, A. R. (1988). "Fourth-order finite-difference P-SV seismograms." *Geophysics*, 53(11), 1425-1436.
10. Madariaga, R. (1976). "Dynamics of an expanding circular fault." *Bulletin of the Seismological Society of America*, 66(3), 639-666.
11. Miyatake, T. (1980). "Numerical simulations of earthquake source process by a three-dimensional crack model." *Journal of Physics of the Earth*, 28(6), 565-598.

12. Moczo, P., Kristek, J., and Bystrický, E. (2000). "Stability and Grid Dispersion of the P-SV 4 th-Order Staggered-Grid Finite-Difference Schemes." *Studia Geophysica et Geodaetica*, 44(3), 381-402.

13. Moczo, P., Kristek, J., Vavrycuk, V., Archuleta, R. J., and Halada, L. (2002). "3D heterogeneous staggered-grid finite-difference modeling of seismic motion with volume harmonic and arithmetic averaging of elastic moduli and densities." *Bulletin of the Seismological Society of America*, 92(8), 3042-3066.

14. Narayan, J. P. (2001). "Site-specific strong ground motion prediction using 2.5-D modelling." *Geophysical Journal International*, 146(2), 269-281.

15. Narayan, J. P. (2005). "Study of basin-edge effects on the ground motion characteristics using 2.5-D modelling." *Pure applied geophysics*, 162(2), 273-289.

16. Narayan, J. P., and Kumar, S. (2010). "Study of effects of focal depth on the characteristics of Rayleigh waves using finite difference method." *Acta Geophysica*, 58(4), 624-644.

17. Narayan, J. P., and Kumar, V. (2014). "Study of combined effects of sediment rheology and basement focusing in an unbounded viscoelastic medium using P-SV-wave finite-difference modelling." *Acta Geophysica*, 62(6), 1214-1245.

18. Oprsal, I., and Zahradnik, J. (2002). "Three-dimensional finite difference method and hybrid modeling of earthquake ground motion." *Journal of Geophysical Research: Solid Earth*, 107(B8).

19. Pitarka, A. (1999). "3D elastic finite-difference modeling of seismic motion using staggered grids with nonuniform spacing." *Bulletin of the Seismological Society of America*, 89(1), 54-68.

20. Virieux, J. (1986). "P-SV wave propagation in heterogeneous media: Velocity-stress finite-difference method." *Geophysics*, 51(4), 889-901.

21. Zahradník, J. í., Moczo, P., and Hron, F. e. (1993). "Testing four elastic finite-difference schemes for behavior at discontinuities." *Bulletin of the Seismological Society of America*, 83(1), 107-129.